

# CTLA-4-expressing ILC3s restrain interleukin-23-mediated inflammation

<https://doi.org/10.1038/s41586-024-07537-3>

Received: 18 April 2023

Accepted: 7 May 2024

Published online: 12 June 2024

 Check for updates

Anees Ahmed<sup>1,2,3</sup>, Ann M. Joseph<sup>1,2,3</sup>, Jordan Zhou<sup>1,2,3</sup>, Veronika Horn<sup>1,2,3</sup>, Jazib Uddin<sup>1,2,3</sup>, Mengze Lyu<sup>1,2,3</sup>, Jeremy Goc<sup>1,2,3</sup>, JRI Live Cell Bank\*, Robbyn E. Sockolow<sup>4</sup>, James B. Wing<sup>5,6,7</sup>, Eric Vivier<sup>8,9,10,11</sup>, Shimon Sakaguchi<sup>5,12</sup> & Gregory F. Sonnenberg<sup>1,2,3</sup> 

Interleukin (IL)-23 is a major mediator and therapeutic target in chronic inflammatory diseases that also elicits tissue protection in the intestine at homeostasis or following acute infection<sup>1–4</sup>. However, the mechanisms that shape these beneficial versus pathological outcomes remain poorly understood. To address this gap in knowledge, we performed single-cell RNA sequencing on all IL-23 receptor-expressing cells in the intestine and their acute response to IL-23, revealing a dominance of T cells and group 3 innate lymphoid cells (ILC3s). Unexpectedly, we identified potent upregulation of the immunoregulatory checkpoint molecule cytotoxic T-lymphocyte-associated antigen-4 (CTLA-4) on ILC3s. This pathway was activated by gut microbes and IL-23 in a FOXO1- and STAT3-dependent manner. Mice lacking CTLA-4 on ILC3s exhibited reduced regulatory T cells, elevated inflammatory T cells and more-severe intestinal inflammation. IL-23 induction of CTLA-4<sup>+</sup> ILC3s was necessary and sufficient to reduce co-stimulatory molecules and increase PD-L1 bioavailability on intestinal myeloid cells. Finally, human ILC3s upregulated CTLA-4 in response to IL-23 or gut inflammation and correlated with immunoregulation in inflammatory bowel disease. These results reveal ILC3-intrinsic CTLA-4 as an essential checkpoint that restrains the pathological outcomes of IL-23, suggesting that disruption of these lymphocytes, which occurs in inflammatory bowel disease<sup>5–7</sup>, contributes to chronic inflammation.

Interleukin (IL)-23 is a heterodimeric cytokine belonging to the IL-12 family, encompassing a shared IL-12p40 subunit and specific IL-23p19 subunit<sup>1,8,9</sup>. Basic mouse models, genetic studies in patients and clinical trials identified that IL-23 is a major mediator of autoimmune and chronic inflammatory disorders, including inflammatory bowel disease (IBD)<sup>9</sup>, psoriasis<sup>10</sup>, rheumatoid arthritis<sup>11</sup> and multiple sclerosis<sup>12</sup>. For example, genome-wide association studies identified single-nucleotide polymorphisms in IL-23 receptor (IL-23R) loci that strongly associate with disease pathogenesis<sup>13,14</sup>, and blocking IL-23 provides therapeutic benefit in a subset of patients<sup>15–17</sup>. However, IL-23 exhibits numerous beneficial, anti-microbial and tissue protective functions. This is particularly evident in the intestine, where IL-23 is produced in response to microbiota colonization, and blockade of IL-23 alters microbiota composition<sup>18</sup>, increases susceptibility to enteric infections<sup>19–21</sup> or, in some cases, exacerbates gut inflammation<sup>22,23</sup>. Furthermore, humans with loss-of-function mutations in *IL23R* are more susceptible to various bacterial and fungal infections at mucosal surfaces<sup>24</sup>. This creates a paradigm that IL-23 mediates both tissue protective and pathological responses, particularly in the intestine,

but the cellular and molecular mechanisms controlling these disparate outcomes remain unclear.

## Mapping IL-23 responses in the small intestine

To comprehensively define the IL-23 pathway, we performed single-cell RNA sequencing (scRNA-seq) of all IL-23R<sup>+</sup> cells in the small intestine of healthy IL-23R-eGFP reporter mice, as well as the acute response of these populations to ex vivo stimulation with IL-23 (Extended Data Fig. 1a). A total of 10,325 unstimulated cells and 8,897 cells with IL-23 stimulation were included in our analyses. Six distinct clusters of IL-23R<sup>+</sup> cells were identified, and each annotated on the basis of select marker genes and visualized by uniform manifold approximation and projection (UMAP). These cell types include well-described subsets of group 3 innate lymphoid cells (ILC3s), γδ T cells, T helper 17 ( $T_{H}17$ ) cells and a minor proliferative cluster with high *Mki67* expression (Fig. 1a,b and Extended Data Fig. 1b,c). The IL-23R<sup>+</sup> ILC3 subsets encompass NKp46<sup>+</sup> or T-bet<sup>+</sup> ILC3s, CCR6<sup>+</sup> lymphoid tissue-inducer-like ILC3s and CCR6<sup>-</sup>NKp46<sup>-</sup> double-negative ILC3s. We validated these results by unbiased flow

<sup>1</sup>Joan and Sanford I. Weill Department of Medicine, Division of Gastroenterology & Hepatology, Weill Cornell Medicine, Cornell University, New York, NY, USA. <sup>2</sup>Department of Microbiology & Immunology, Weill Cornell Medicine, Cornell University, New York, NY, USA. <sup>3</sup>Jill Roberts Institute for Research in Inflammatory Bowel Disease, Weill Cornell Medicine, Cornell University, New York, NY, USA. <sup>4</sup>Department of Pediatrics, Division of Gastroenterology, Hepatology, & Nutrition, Weill Cornell Medicine, Cornell University, New York, NY, USA. <sup>5</sup>Laboratory of Experimental Immunology, World Premier International Immunology Frontier Research Center, Osaka University, Suita, Japan. <sup>6</sup>Laboratory of Human Single Cell Immunology, WPI iReC, Osaka University, Suita, Japan. <sup>7</sup>Human Single Cell Immunology Team, Center for Infectious Disease Education and Research, Osaka University, Suita, Japan. <sup>8</sup>Innate Pharma Research Laboratories, Innate Pharma, Marseille, France. <sup>9</sup>Aix Marseille University, CNRS, INSERM, CIML, Marseille, France. <sup>10</sup>APHM, Hôpital de la Timone, Marseille-Immunopôle, Marseille, France. <sup>11</sup>Paris Saclay Cancer Cluster, Villejuif, France. <sup>12</sup>Department of Experimental Pathology, Institute for Frontier Medical Sciences, Kyoto University, Kyoto, Japan. \*A list of authors and their affiliations appears at the end of the paper.  e-mail: gfsonnenberg@med.cornell.edu

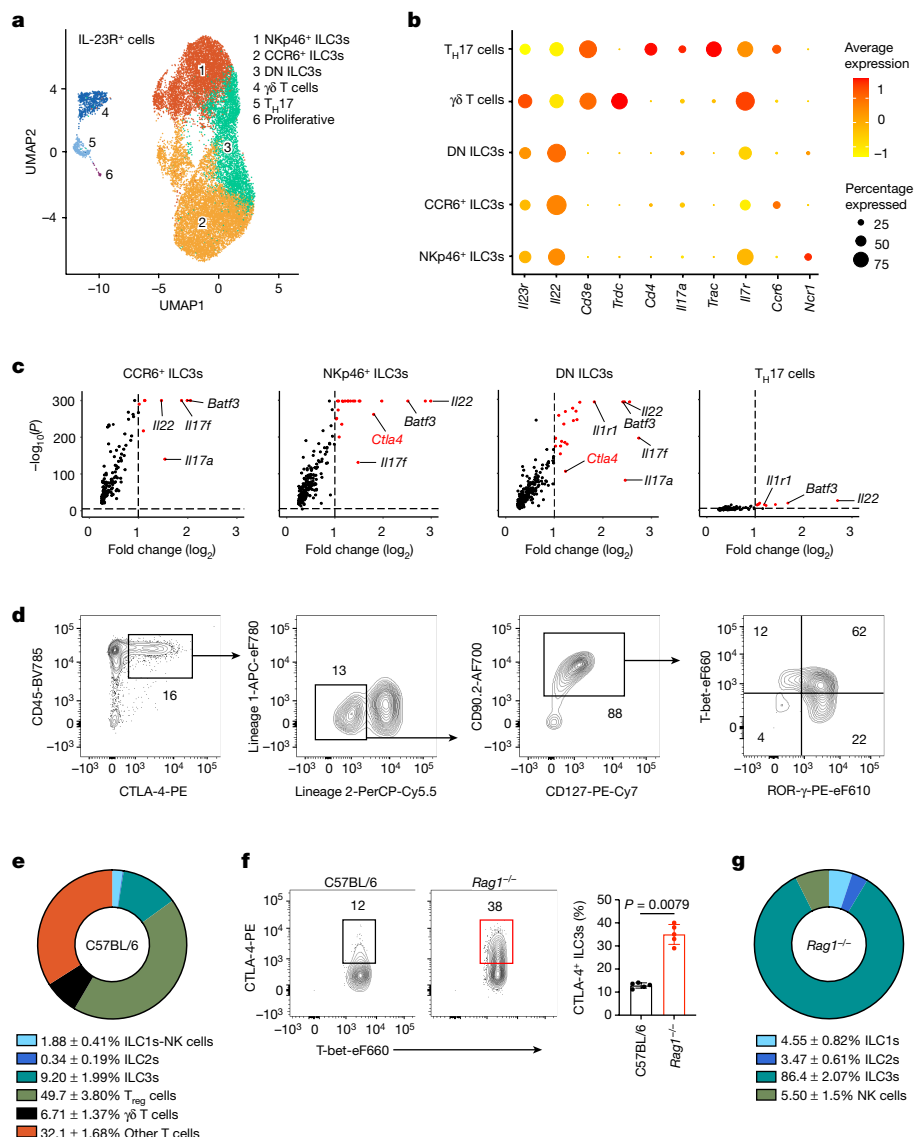


**Fig. 1 | A single-cell atlas of IL-23 responses in the small intestine identifies CTLA-4<sup>+</sup> ILC3s.** **a**, UMAP plot of scRNA-seq data encompassing IL-23R<sup>+</sup> immune cells from small intestine lamina propria of IL-23R-eGFP mice. **b**, Dot plots showing the mean expression of the indicated genes among different clusters. **c**, Volcano plots of differentially expressed genes in scRNA-seq dataset of IL-23R<sup>+</sup> immune cells from small intestine lamina propria of IL-23R-eGFP mice before or after IL-23 stimulation. **d,e**, Flow cytometry plots (**d**) and donut plot (**e**) with final frequencies of different CTLA-4<sup>+</sup> cells in small intestine lamina propria of C57BL/6 mice ( $n = 4$  mice). Lineage 1, CD11b, CD11c and B220; lineage

2, CD3 $\epsilon$ , CD5, CD8 $\alpha$  and TCR $\gamma\delta$ . **f**, Flow cytometry plots with graph displaying the frequency of CTLA-4<sup>+</sup> ILC3s (percentage of total ILC3s) in small intestine lamina propria of C57BL/6 and *Rag1*<sup>-/-</sup> mice ( $n = 5$  mice). **g**, Donut plot with final frequencies of different CTLA-4<sup>+</sup> cells in small intestine lamina propria of *Rag1*<sup>-/-</sup> mice ( $n = 4$  mice). Data in **d–g** are representative of two or three independent experiments with similar results, shown as mean  $\pm$  s.d. The statistics in **c** were obtained by the Wilcoxon test as implemented by Seurat. The statistic in **f** was calculated by Mann-Whitney *U*-test (unpaired, two-tailed). DN, double-negative; NK, natural killer.

cytometry using IL-23R-eGFP mice and quantitatively determined selective expression of IL-23R in these cells, as well as in the large intestine of naive mice or following *Citrobacter rodentium* infection (Extended Data Fig. 2a–c). After acute IL-23 stimulation, we observed robust transcriptional changes predominantly among the ILC3 subsets and modest transcriptional changes in T cells (Fig. 1c and Extended Data Fig. 3a,b). Several expected transcriptional changes were observed, including engagement of IL-17 and IL-22; however, we also observed potent upregulation of the immunoregulatory checkpoint molecule cytotoxic T-lymphocyte-associated antigen-4 (CTLA-4) among the NKp46<sup>+</sup> and double-negative ILC3 subsets, as well as in  $\gamma\delta$  T cells, to a lesser extent (Fig. 1c and Extended Data Fig. 3a,b). Given this unexpected finding, we next profiled cellular sources of CTLA-4 protein by unbiased flow cytometry in the healthy C57BL/6 mouse small intestine.

Regulatory T (T<sub>reg</sub>) cells are the dominant cell type expressing CTLA-4; however, we also found that a sizable proportion of CTLA-4<sup>+</sup> cells lack lineage markers and are ILC3s (Fig. 1d,e). NKp46<sup>+</sup> ILC3s express the most CTLA-4 relative to other innate lymphocytes (Extended Data Fig. 4a,b). A majority of the CTLA-4<sup>+</sup> ILC3s co-express T-bet, and, consistent with previous reports of IL-23-dependent hyperactivation in the absence of adaptive immunity<sup>25,26</sup>, ILC3s express significantly more CTLA-4 in the small intestine of *Rag1*<sup>-/-</sup> mice (Fig. 1f). In this setting, ILC3s are the dominant CTLA-4<sup>+</sup> cell type in the small intestine (Fig. 1g and Extended Data Fig. 4c). These data provide a comprehensive single-cell atlas of all IL-23R<sup>+</sup> immune cells in the healthy mammalian intestine and following acute IL-23 activation, which revealed a previously unappreciated upregulation of the immunoregulatory checkpoint molecule CTLA-4 on ILC3s.

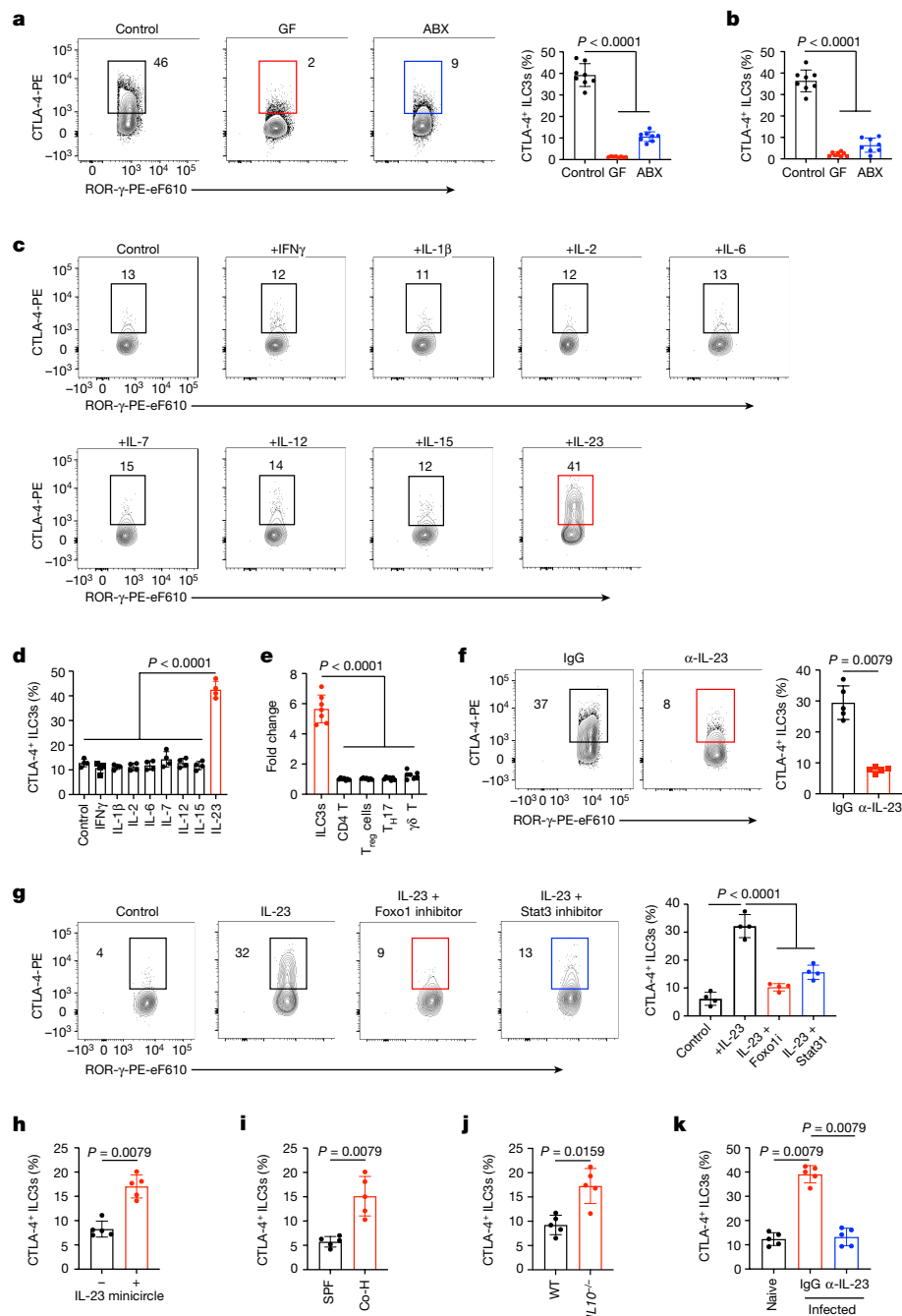


**Fig. 2 | Microbial exposure elicits IL-23 to upregulate CTLA-4 on ILC3s.**  
**a,b**, Flow cytometry plots with graph of CTLA-4<sup>+</sup> ILC3 frequency (percentage of total ILC3s) in large intestine (a) and small intestine (b) lamina propria of SPF, germ-free (GF) and SPF *Rag1*<sup>-/-</sup> mice treated with antibiotics (ABX) ( $n = 8$  mice).  
**c,d**, Flow cytometry plots (c) and graph of CTLA-4<sup>+</sup> ILC3 frequency (d) (percentage of total ILC3s) in small intestine lamina propria of SPF mice ex vivo stimulated with indicated cytokines ( $n = 4$  mice).  
**e**, Fold change in CTLA-4 protein in different immune cells from lamina propria of SPF mice ex vivo cultured for 4 h with IL-23 ( $n = 7$  mice).  
**f**, Flow cytometry plots with graph of CTLA-4<sup>+</sup> ILC3 frequency (percentage of total ILC3s) in small intestine lamina propria of *Rag1*<sup>-/-</sup> mice treated with IgG control or anti-IL-23 antibody ( $n = 5$  mice).  
**g**, Flow cytometry plots of CTLA-4<sup>+</sup> ILC3s (percentage of total ILC3s) in small intestine lamina propria of SPF mice cultured ex vivo in different conditions ( $n = 4$  mice).

lamina propria of SPF mice cultured ex vivo in different conditions ( $n = 4$  mice).  
**h–k**, Graphs showing frequency of CTLA-4<sup>+</sup> ILC3s (percentage of total ILC3s) in large intestine lamina propria of mice injected with or without IL-23 minicircle (h); SPF mice co-housed (Co-H) with or without pet store mice (i); C57BL/6 wild-type (WT) and *IL10*<sup>-/-</sup> mice (j); or mice infected with *C. rodentium* and treated with IgG control or anti-IL-23 antibody (k) ( $n = 5$  mice). Data in a, b and e were pooled from two independent experiments with similar results, shown as mean  $\pm$  s.d. Data in c, d and f–k are representative of two independent experiments, shown as mean  $\pm$  s.d. The statistics in a, b, d, e and g were calculated by one-way analysis of variance (ANOVA) with Dunnett's multiple comparisons. The statistics in f and h–k were calculated by Mann–Whitney U-test (unpaired, two-tailed).

### A microbe–IL-23 axis drives CTLA-4<sup>+</sup> ILC3s

The intestinal microbiota is required for the proper development and function of ILC3s<sup>27,28</sup>. To investigate whether intestinal microbiota is required for ILC3-intrinsic CTLA-4, we profiled the large

and small intestine of mice that are specific-pathogen-free (SPF), germ-free or exposed to broad-spectrum antibiotics. Notably, both germ-free *Rag1*<sup>-/-</sup> mice and SPF *Rag1*<sup>-/-</sup> mice that were exposed to broad-spectrum antibiotics displayed a significant reduction of CTLA-4 protein in ILC3s relative to controls (Fig. 2a,b). Limited staining of

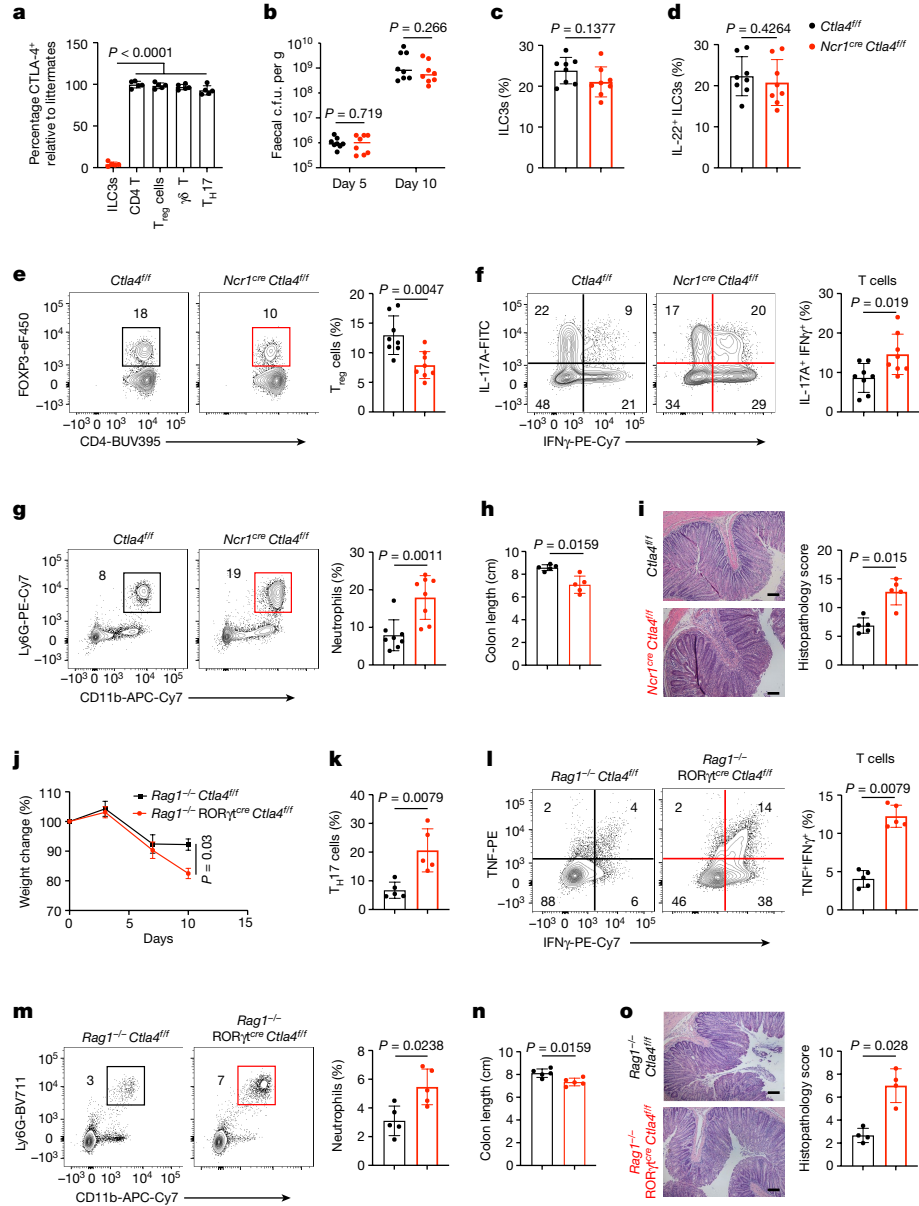


**Fig. 3 | CTLA-4<sup>+</sup> ILC3s restrain IL-23-dependent gut inflammation.**

**a**, Percentage of CTLA-4<sup>+</sup> immune cells ( $n = 5$  mice). **b**, Mice were infected with *C. rodentium*, and the graph shows faecal bacteria at the indicated days post infection (dpi) ( $n = 8$  mice). **c,d**, Immune cells in large intestine at 14 dpi. Graphs displaying frequency of ILC3s (**c**) (percentage of Lin<sup>-</sup>CD90<sup>+</sup>CD127<sup>+</sup> cells) and IL-22<sup>+</sup> ILC3s (**d**) (percentage of total ILC3s;  $n = 8$  mice). **e**, Flow cytometry plots with graph of T<sub>reg</sub> cell frequency among CD4<sup>+</sup> T cells ( $n = 8$  mice). **f**, Flow cytometry plots with graph of IL-17A<sup>+</sup> IFN $\gamma$ <sup>+</sup> cell frequency among CD4<sup>+</sup> T cells ( $n = 8$  mice). **g,h**, Flow cytometry plots with graph of neutrophil frequency among CD45<sup>+</sup> cells (**g**) ( $n = 8$  mice) and with colon lengths at 14 dpi (**h**) ( $n = 5$  mice). **i**, H&E staining and histopathology score of distal colon at 14 dpi ( $n = 5$  mice). Scale bars, 50  $\mu$ m. Naive CD4<sup>+</sup> T cells were transferred to recipient mice

and analysed 11 d later. **j**, Graph of weight loss ( $n = 5$  mice). **k**, Immune cells in large intestine with graph showing T<sub>H</sub>17 cell frequency among CD4<sup>+</sup> T cells ( $n = 5$  mice). **l**, Flow cytometry plots with TNF $\gamma$ IFN $\gamma$ <sup>+</sup> cell frequency among CD4<sup>+</sup> T cells ( $n = 5$  mice). **m,n**, Flow cytometry plots with graph of neutrophil frequency among CD45<sup>+</sup> cells (**m**) ( $n = 5$  mice) and with colon length (**n**) ( $n = 5$  mice). **o**, H&E staining and histopathology score of distal colon ( $n = 4$  mice). Scale bars, 50  $\mu$ m. Data in **a–g** and **j–o** were pooled from two independent experiments. All data are shown as mean  $\pm$  s.d. The statistics in **a** were calculated by one-way ANOVA with Dunnett's multiple comparisons and in **b–o** by Mann-Whitney *U*-test (unpaired, two-tailed). c.f.u., colony-forming unit; H&E, haematoxylin and eosin.

microbiota-dependent CTLA-4 was observed in group 1 innate lymphoid cells (ILC1s) and natural killer cells (Extended Data Fig. 5a,b). To determine the signals that directly promote CTLA-4 in ILC3s, we stimulated intestinal cells with canonical activators interferon- $\gamma$  (IFN $\gamma$ ), IL-1 $\beta$ , IL-2, IL-6, IL-7, IL-12, IL-15 and IL-23 (refs. 27,28). Among these, IL-23 robustly and selectively induced CTLA-4 protein in ILC3s, whereas IL-12 induced CTLA-4 in ILC1s (Fig. 2c,d and Extended Data Fig. 5c). IL-23 potently upregulated CTLA-4 in ILC3s, with modest changes in  $\gamma$ 6 T cells, and this was not sufficient to modulate CTLA-4 in T<sub>reg</sub> cells

or T<sub>H</sub>17 cells (Fig. 2e and Extended Data Fig. 5c). Furthermore, the frequency of CTLA-4<sup>+</sup> ILC3s was significantly reduced after in vivo blockade of IL-23 using a monoclonal antibody (Fig. 2f). FOXO1 and STAT3 are two downstream pathways engaged by IL-23R signalling and linked to CTLA-4 expression in T<sub>reg</sub> cells<sup>29,30</sup>. We found that inhibition of either FOXO1 or STAT3 activation significantly limited IL-23-mediated induction of CTLA-4 in ILC3s (Fig. 2g). We next investigated whether diverse microbial encounters or chronic inflammatory environments regulate ILC3-intrinsic CTLA-4. Notably, overexpression of IL-23 in mice with

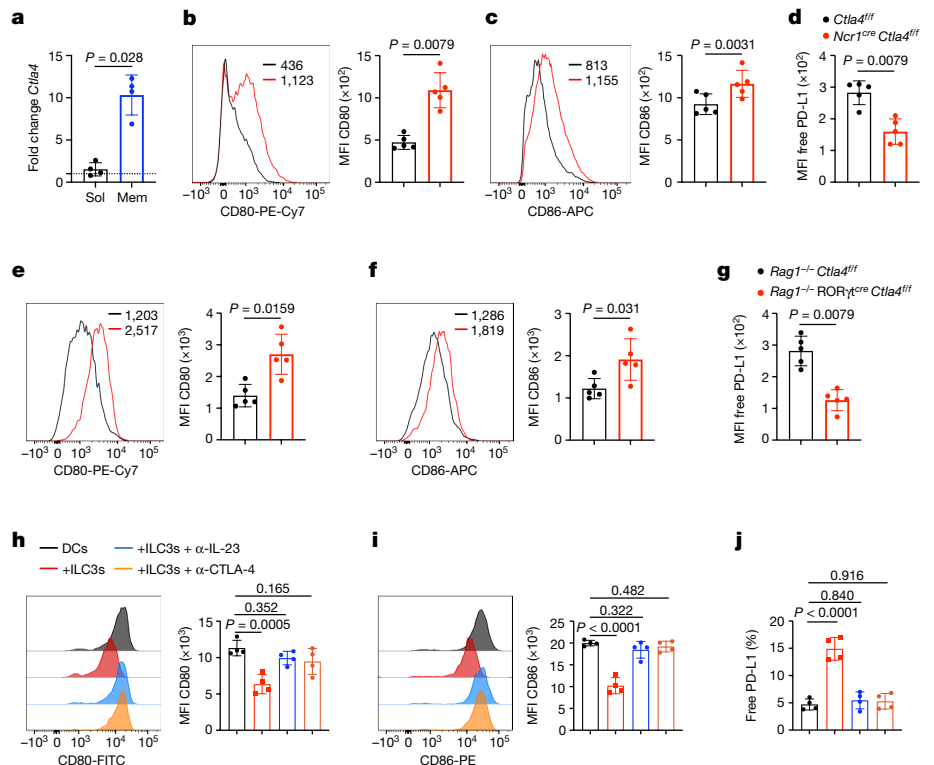


**Fig. 4 | CTLA-4<sup>+</sup> ILC3s regulate co-stimulatory and inhibitory checkpoints on myeloid cells in the gut.** **a**, Relative soluble (Sol) and membrane (Mem) *Ctla4* transcripts in the sort-purified ILC3s stimulated with IL-23 ( $n = 4$  mice). The dotted line represents fold change of 1. Mice were orally infected with *C. rodentium*, and myeloid cells in large intestine lamina propria were analysed at 14 dpi. **b-d**, Flow cytometry plots with graph of MFI for CD80 (**b**) and CD86 (**c**) and free PD-L1 (**d**) expression on myeloid cells gated as  $\text{CD11c}^{\text{hi}} \text{MHCII}^{\text{hi}}$  ( $n = 5$  mice). Naive CD4<sup>+</sup> T cells were adoptively transferred to recipient mice and myeloid cells in large intestine lamina propria were analysed at day 11 post transfer. **e-g**, Flow cytometry plots with graph of MFI for CD80 (**e**) and CD86 (**f**) on myeloid cells gated as  $\text{CD11c}^{\text{hi}} \text{MHCII}^{\text{hi}}$  from *Rag1<sup>-/-</sup> Ctla4<sup>fl/fl</sup>* (black) and *Rag1<sup>-/-</sup> ROR $\gamma$  *cre* Ctla4<sup>fl/fl</sup>* (red) mice. **h-j**, Graph of free PD-L1 frequency on myeloid cells gated as  $\text{CD11c}^{\text{hi}} \text{MHCII}^{\text{hi}}$  ( $n = 4$  mice). Data in **a-j** are representative of two or three independent experiments with similar results and are shown as mean  $\pm$  s.d. The statistics in **a-j** were obtained by Mann-Whitney *U*-test (unpaired, two-tailed). MFI, mean fluorescence intensity.

and free PD-L1 (**g**) expression on myeloid cells gated as  $\text{CD11c}^{\text{hi}} \text{MHCII}^{\text{hi}}$  ( $n = 5$  mice). Sorted ILC3s and myeloid cells from the large intestine lamina propria of C57BL/6 mice were co-cultured with heat-killed *C. rodentium* for 20 h in different conditions. **h-i**, Flow cytometry plots with graph of MFI for CD80 (**h**) and CD86 (**i**) expression on myeloid cells gated as  $\text{CD11c}^{\text{hi}} \text{MHCII}^{\text{hi}}$  ( $n = 4$  mice). **j**, Graph of free PD-L1 frequency on myeloid cells gated as  $\text{CD11c}^{\text{hi}} \text{MHCII}^{\text{hi}}$  ( $n = 4$  mice). Data in **a-j** are representative of two or three independent experiments with similar results and are shown as mean  $\pm$  s.d. The statistics in **a-j** were obtained by Mann-Whitney *U*-test (unpaired, two-tailed). MFI, mean fluorescence intensity.

a minicircle vector resulted in significantly increased ILC3-intrinsic CTLA-4 in the large intestine (Fig. 2h). ILC3-specific CTLA-4 was also upregulated in the large intestine following exposure of SPF mice to diverse microbes by co-housing with pet store mice, in the context of IL-10 deficiency and spontaneous gut inflammation, or after infection with *C. rodentium*, in an IL-23-dependent manner (Fig. 2i-k). These data demonstrate that microbiota colonization of the intestine and associated induction of IL-23 support the presence of CTLA-4<sup>+</sup> ILC3s at homeostasis in a FOXO1- and STAT3-dependent manner, and that this pathway is further engaged in the context of diverse microbial exposure, enteric infection or chronic inflammation.

### CTLA-4<sup>+</sup> ILC3s restrain gut inflammation

To explore the functional importance of this pathway, we generated mice with a deletion of CTLA-4 in ILC3s by crossing NKp46-cre mice (*Ncr1<sup>cre</sup>*) with mice expressing *loxP*-flanked (floxed) *Ctla4* (*Ctla4<sup>fl/fl</sup>*). This approach was selected because CTLA-4 is dominantly expressed on the NKp46<sup>+</sup> ILC3 subset, and, with unbiased gating on all NKp46<sup>+</sup> cells, we observe that ILC3s are the major subtype that is CTLA-4<sup>+</sup> at homeostasis and following *C. rodentium* infection (Extended Data Fig. 6a,b). The resulting *Ncr1<sup>cre</sup> Ctla4<sup>fl/fl</sup>* mice demonstrated a deletion of CTLA-4 on T-bet<sup>+</sup> ILC3s, without impacting CTLA-4 on T cells (Fig. 3a). These mice exhibit comparable frequencies, subset distribution and cytokine production among various immune cells in the large intestine at homeostasis (Extended Data Fig. 6c-g). We next

investigated the role of CTLA-4<sup>+</sup> ILC3s using the enteric pathogen *C. rodentium*, which induces potent upregulation of IL-23 to drive optimal immunity<sup>19–21</sup>. In this context, there was no significant difference of pathogen burden, or in the frequencies of ILC3s and IL-22 production, in the large intestine of *Ncr1<sup>cre</sup> Ctla4<sup>fl/fl</sup>* mice relative to littermate controls (Fig. 3b-d). IL-23 is also linked to reducing the stability and functionality of T<sub>reg</sub> cell responses<sup>23,31,32</sup>. Therefore, despite this intact immunity to *C. rodentium*, we profiled the adaptive immune response during infection and found a significant reduction in the frequency of T<sub>reg</sub> cells and significant elevation of pro-inflammatory T cells that co-produce IFN $\gamma$  and IL-17A in the colon of mice lacking CTLA-4<sup>+</sup> ILC3s relative to littermate controls (Fig. 3e,f). Consistent with this imbalance in effector and regulatory T cell responses, *Ncr1<sup>cre</sup> Ctla4<sup>fl/fl</sup>* mice exhibited significantly elevated colonic neutrophils, shorter colon length and increased histological evidence of intestinal inflammation (Fig. 3g-i). Natural killer cells and ILC1s had minimal levels of CTLA-4 in the healthy gut that were unchanged during *C. rodentium* infection (Extended Data Fig. 7a). Depletion of these cells, but not ILC3s, with an anti-NK1.1 antibody during *C. rodentium* infection did not alter the inflammatory outcomes of mice (Extended Data Fig. 7b-f). Loss of one copy of NKp46 or *Ncr1* also did not impact inflammation in the large intestine following *C. rodentium* infection (Extended Data Fig. 8a-d). These results collectively indicate that CTLA-4 is upregulated on ILC3s in response to an enteric pathogen and IL-23 to subsequently restrain inflammatory T cell responses and promote immunoregulation.

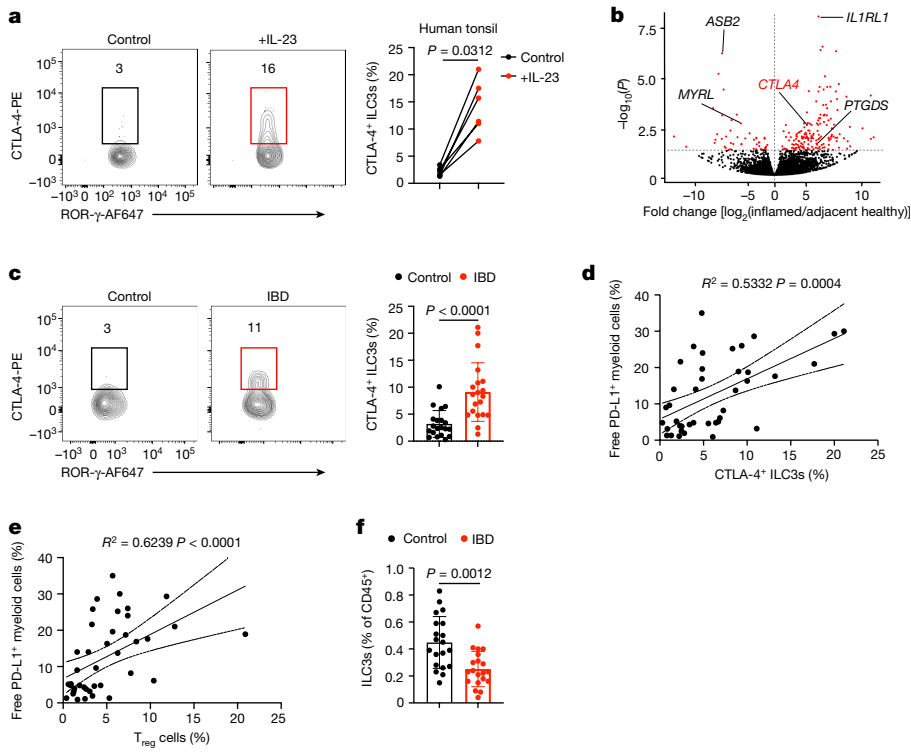


**Fig. 5 | IL-23 upregulates CTLA-4<sup>+</sup> ILC3s in humans and this axis is altered in IBD.** **a**, Flow cytometry plots with graph of CTLA-4<sup>+</sup> ILC3 frequency (percentage of total ILC3s) from human tonsils stimulated for 6 h with or without recombinant human IL-23 ( $n = 6$  human samples). **b**, Volcano plot of differentially expressed genes in bulk RNA sequencing dataset of ILC3s sorted from the inflamed or normal adjacent intestinal tissue of patients with IBD. Immune cells were isolated from intestinal biopsies of 20 healthy human controls or patients with Crohn's disease (CD). **c**, Flow cytometry plots with graph of CTLA-4<sup>+</sup> ILC3 frequency gated as CD45<sup>+</sup>Lin<sup>-</sup>CD127<sup>+</sup>ROR $\gamma$ T cells (percentage of total ILC3s). **d**, Frequency of CTLA-4<sup>+</sup> ILC3s (percentage of total ILC3s) was correlated with frequency of free PD-L1<sup>+</sup> myeloid cells (percentage of total myeloid cells) gated as CD45<sup>+</sup>CD11c<sup>+</sup>MHCII<sup>+</sup> cells ( $n = 20$  non-IBD human

controls;  $n = 20$  human patients with CD). **e**, Frequency of free PD-L1<sup>+</sup> myeloid cells (percentage of total myeloid cells) was correlated with T<sub>reg</sub> cell frequency gated as CD45<sup>+</sup>CD3<sup>+</sup>CD4<sup>+</sup>FOXP3<sup>+</sup> of CD4<sup>+</sup>T cells ( $n = 20$  non-IBD human controls;  $n = 20$  human patients with CD). **f**, Graph of ILC3 frequency gated as CD45<sup>+</sup>Lin<sup>-</sup>CD127<sup>+</sup>ROR $\gamma$ T cells relative to total CD45<sup>+</sup> cells ( $n = 20$  non-IBD human controls;  $n = 20$  human patients with CD). The statistics in **a** were calculated using Wilcoxon matched-pairs test (paired, two-tailed). The statistics in **b** were calculated using the Wald test within DESeq2. The statistics in **c** and **f** were calculated by Mann–Whitney *U*-test (unpaired, two-tailed). Correlative analyses in **d** and **e** were calculated by non-parametric Spearman correlation. Data in **a** are representative of two independent experiments, shown as mean  $\pm$  s.d.

To validate this finding, we also generated *Rag1*<sup>-/-</sup> ROR $\gamma$ T<sup>cre</sup> *Ctla4*<sup>ff</sup> mice and examined the functional importance of ILC3-specific CTLA-4 in models of intestinal inflammation induced by anti-CD40 agonistic antibody<sup>33</sup> or naive T cell transfer<sup>34</sup>. Interestingly, despite robust CTLA-4 deletion in ILC3s, the agonistic anti-CD40 model in *Rag1*<sup>-/-</sup> ROR $\gamma$ T<sup>cre</sup> *Ctla4*<sup>ff</sup> mice revealed comparable ILC3 responses, as well as parameters of intestinal inflammation, including leukocyte infiltration and colonic shortening, relative to littermate controls (Extended Data Fig. 8e–i). This demonstrates that ILC3-specific CTLA-4 is dispensable when T cells are absent and is consistent with the intact innate immunity observed in this model and the *C. rodentium* infection model. By contrast, during the naive T cell transfer model, which is driven by adaptive immunity and dependent on IL-23 (ref. 34), we observed that mice lacking ILC3-specific CTLA-4 exhibit significantly greater weight loss, frequency of T<sub>H</sub>17 cells, production of TNF and IFN $\gamma$  from colonic T cells, and colonic neutrophil infiltration; shorter colon length; and increased histological evidence of intestinal inflammation relative to littermate controls (Fig. 3j–o). These data demonstrate that ILC3-specific CTLA-4 is necessary to restrain inflammatory T cell responses and promote immunoregulation in mouse models of IL-23-driven colitis.

### CTLA-4<sup>+</sup> ILC3s shape gut co-stimulation

CTLA-4, particularly on T<sub>reg</sub> cells, mediates critical immunosuppressive functions<sup>35,36</sup>. This occurs in part through CTLA-4-dependent

trogocytosis of CD80 and CD86 on myeloid cells, restricting the activation of effector T cells in autoimmunity and chronic inflammation<sup>37,38</sup>. Therefore, we next examined whether CTLA-4<sup>+</sup> ILC3s modulate co-stimulatory molecules on intestinal myeloid cells and in response to IL-23. We found that IL-23 primarily drives upregulation of the membrane-bound compared with the soluble form of CTLA-4 on ILC3s (Fig. 4a). We also profiled co-stimulatory molecules on large intestine myeloid cells following *C. rodentium* infection and found that mice lacking CTLA-4<sup>+</sup> ILC3s exhibit significantly increased levels of CD80 and CD86 on myeloid cells relative to littermate controls (Fig. 4b,c). Recent seminal studies indicate that CD80 interacts with PD-L1 in a *cis*-manner on myeloid cells, which prevents PD-L1 on myeloid cells from interacting with PD-1 on other cell types<sup>39,40</sup>. It was recently demonstrated that CTLA-4<sup>+</sup> T<sub>reg</sub> cells decrease this *cis*-interaction through the trogocytosis of CD80 to increase the bioavailability of free PD-L1 on myeloid cells<sup>39</sup>, whereas other earlier studies indicate that PD-L1 signals from myeloid cells support the generation or maintenance of PD-1<sup>+</sup> T<sub>reg</sub> cells<sup>41,42</sup>. Consistent with this, we found that with the increase in co-stimulatory molecules, there was significant reduction in the bioavailability of free PD-L1 on myeloid cells from mice lacking CTLA-4<sup>+</sup> ILC3s during *C. rodentium* infection (Fig. 4d). Similarly, *Rag1*<sup>-/-</sup> ROR $\gamma$ T<sup>cre</sup> *Ctla4*<sup>ff</sup> mice lacking CTLA-4<sup>+</sup> ILC3s and receiving a naive T cell transfer exhibit significantly increased levels of CD80 and CD86 with a significant reduction in the bioavailability of free PD-L1 on myeloid cells from the large intestine relative to littermate controls (Fig. 4e–g). We next asked

# Article

whether CTLA-4 from ILC3s is sufficient to impart these outcomes using an ex vivo co-culture system. Notably, we found that co-culture of ILC3s and myeloid cells from the large intestine following exposure to heat-killed *C. rodentium*, or in the presence of recombinant IL-23, resulted in a significant reduction of CD80 and CD86 on myeloid cells (Fig. 4h,i and Extended Data Fig. 9a,b). In both settings, blockade of either IL-23 or CTLA-4 reversed this downregulation of CD80 and CD86 on intestinal myeloid cells (Fig. 4h,i and Extended Data Fig. 9a,b). ILC3 co-culture also resulted in significantly increased bioavailability of PD-L1 on myeloid cells in both a CTLA-4- and a IL-23-dependent manner (Fig. 4j and Extended Data Fig. 9c). These data demonstrate that IL-23 drives upregulation of CTLA-4 on ILC3s that is necessary and sufficient to reduce co-stimulatory molecules on gut myeloid cells and increase bioavailability of the key immunoregulatory molecule PD-L1.

## CTLA-4<sup>+</sup> ILC3s are altered in IBD

We next explored for clinical relevance and whether this pathway is functional in humans. We found in an ex vivo culture that IL-23 was sufficient to significantly upregulate CTLA-4 in human ILC3s derived from tonsils (Fig. 5a). To explore this pathway in a disease setting, we performed bulk RNA sequencing on ILC3s sorted from the inflamed intestine or matched adjacent non-inflamed intestine samples that were resected from patients with IBD, encompassing both Crohn's disease and ulcerative colitis (Supplementary Table 1). We identified 254 genes that were upregulated and 79 genes that were downregulated in ILC3s from inflamed tissue relative to adjacent non-inflamed intestine, and, interestingly, among these differentially upregulated genes, a notable significant increase in *CTLA4* was observed in ILC3s (Fig. 5b). We validated this by performing profiling of intestinal biopsies from patients with IBD versus age- and gender-matched controls (Supplementary Table 2). We observed a significantly increased frequency of CTLA-4<sup>+</sup> ILC3s in patients with Crohn's disease relative to healthy controls (Fig. 5c and Extended Data Fig. 9d). Notably, we identified a significant positive correlation between the frequencies of CTLA-4<sup>+</sup> ILC3s and free PD-L1<sup>+</sup> intestinal myeloid cells within the same biopsies of patients with IBD (Fig. 5d). Furthermore, the abundance of free PD-L1 on myeloid cells exhibited a significant positive correlation with T<sub>reg</sub> cell frequencies (Fig. 5e). These datasets reveal that human ILC3s upregulate CTLA-4 in response to IL-23 or in the inflamed intestine, and that this pathway correlates with immunoregulatory checkpoints during disease. However, as previously reported<sup>5–7</sup>, we also observed a significantly reduced frequency of overall ILC3s in intestinal biopsies from patients with Crohn's disease relative to those from healthy controls (Fig. 5f), indicating that this pathway can become compromised in patients with IBD.

## Discussion

Here we identify ILC3s as a critical link between potent IL-23-driven inflammatory and immunoregulatory checkpoints in the intestine. This provokes a model whereby microbial exposure induces IL-23 to subsequently upregulate CTLA-4 on ILC3s, which then supports immunoregulation by reducing co-stimulatory molecules, CD80 and CD86, and increasing bioavailability of PD-L1 on myeloid cells (Extended Data Fig. 10). Impairment of this pathway manifests in a substantial imbalance of effector and regulatory T cell responses and enhanced intestinal inflammation. This is a key conceptual advance in our understanding of how IL-23 functions at homeostasis and in a tissue protective manner following exposure to diverse microbes. It is entirely distinct from our previous studies detailing how IL-2-producing ILC3s support T<sub>reg</sub> cells in the small intestine<sup>7</sup>, or how antigen-presenting ILC3s instruct differentiation of microbiota-specific T<sub>reg</sub> cells<sup>43</sup>, both of which occur at steady state and are independent of IL-23. Furthermore, it indicates that ILC3-specific CTLA-4 counteracts the appreciated inhibitory roles of

IL-23 on T<sub>reg</sub> cells<sup>23,31,32</sup>, probably through PD-L1 (ref. 41). This is particularly important in the gastrointestinal tract, which is regularly colonized with beneficial microbiota, opportunistic microbes or enteric pathogens that induce robust and local IL-23 production. Therefore, these tissue-resident ILC3 responses critically balance this pro-inflammatory cytokine to maintain gut homeostasis. It remains possible that CTLA-4 is functionally important to other innate or innate-like lymphocytes following exposure to different signalling cues. ILC3s are known to be depleted from the gut in the setting of chronic IL-23 exposure in mouse models<sup>44,45</sup>, or in chronic diseases such as IBD<sup>5–7,43,46</sup>, colorectal cancer<sup>47</sup> and various infections<sup>48</sup>. Therefore, although we find that this pathway is functional in humans, disrupted engagement of IL-23-dependent CTLA-4<sup>+</sup> ILC3s could shift the balance from immunoregulation to inflammation, which may represent a key transition that supports the pathogenesis of chronic inflammatory diseases. Finally, this study also informs on the use of CTLA-4 blockade in the context of cancer immunotherapy, which can provide a substantial therapeutic benefit but often manifests in checkpoint-induced colitis as an immune-related adverse event<sup>49,50</sup>. Advances to support CTLA-4<sup>+</sup> ILC3s and engagement of the PD-L1 pathway represent an opportunity to counteract aberrant IL-23-driven chronic inflammation.

## Online content

Any methods, additional references, Nature Portfolio reporting summaries, source data, extended data, supplementary information, acknowledgements, peer review information; details of author contributions and competing interests; and statements of data and code availability are available at <https://doi.org/10.1038/s41586-024-07537-3>.

1. Abraham, C. & Cho, J. H. IL-23 and autoimmunity: new insights into the pathogenesis of inflammatory bowel disease. *Annu. Rev. Med.* **60**, 97–110 (2009).
2. Maloy, K. J. & Powrie, F. Intestinal homeostasis and its breakdown in inflammatory bowel disease. *Nature* **474**, 298–306 (2011).
3. Maynard, C. L., Elson, C. O., Hatton, R. D. & Weaver, C. T. Reciprocal interactions of the intestinal microbiota and immune system. *Nature* **489**, 231–241 (2012).
4. Fragogiannis, G. E., Siebert, S. & McInnes, I. B. Therapeutic targeting of IL-17 and IL-23 cytokines in immune-mediated diseases. *Annu. Rev. Med.* **67**, 337–353 (2016).
5. Bernink, J. H. et al. Human type 1 innate lymphoid cells accumulate in inflamed mucosal tissues. *Nat. Immunol.* **14**, 221–229 (2013).
6. Takayama, T. et al. Imbalance of NKp44<sup>+</sup>NKp46<sup>−</sup> and NKp44<sup>−</sup>NKp46<sup>+</sup> natural killer cells in the intestinal mucosa of patients with Crohn's disease. *Gastroenterology* **139**, 882–892 (2010).
7. Zhou, L. et al. Innate lymphoid cells support regulatory T cells in the intestine through interleukin-2. *Nature* **568**, 405–409 (2019).
8. Oppmann, B. et al. Novel p19 protein engages IL-12p40 to form a cytokine, IL-23, with biological activities similar as well as distinct from IL-12. *Immunity* **13**, 715–725 (2000).
9. Neurath, M. F. IL-23: a master regulator in Crohn disease. *Nat. Med.* **13**, 26–28 (2007).
10. Krueger, G. G. et al. A human interleukin-12/23 monoclonal antibody for the treatment of psoriasis. *N. Engl. J. Med.* **356**, 580–592 (2007).
11. Lubberts, E. The IL-23-IL-17 axis in inflammatory arthritis. *Nat. Rev. Rheumatol.* **11**, 415–429 (2015).
12. Cua, D. J. et al. Interleukin-23 rather than interleukin-12 is the critical cytokine for autoimmune inflammation of the brain. *Nature* **421**, 744–748 (2003).
13. Duerr, R. H. et al. A genome-wide association study identifies *IL23R* as an inflammatory bowel disease gene. *Science* **314**, 1461–1463 (2006).
14. The Wellcome Trust Case Control Consortium. Genome-wide association study of 14,000 cases of seven common diseases and 3,000 shared controls. *Nature* **447**, 661–678 (2007).
15. D'Haens, G. et al. Risankizumab as induction therapy for Crohn's disease: results from the phase 3 ADVANCE and MOTIVATE induction trials. *Lancet* **399**, 2015–2030 (2022).
16. Feagan, B. G. et al. Ustekinumab as induction and maintenance therapy for Crohn's disease. *N. Engl. J. Med.* **375**, 1946–1960 (2016).
17. Sands, B. E. et al. Ustekinumab as induction and maintenance therapy for ulcerative colitis. *N. Engl. J. Med.* **381**, 1201–1214 (2019).
18. Shih, V. F. et al. Homeostatic IL-23 receptor signaling limits Th17 response through IL-22-mediated containment of commensal microbiota. *Proc. Natl. Acad. Sci. USA* **111**, 13942–13947 (2014).
19. Mangan, P. R. et al. Transforming growth factor-β induces development of the T<sub>H</sub>17 lineage. *Nature* **441**, 231–234 (2006).
20. Zheng, Y. et al. Interleukin-22 mediates early host defense against attaching and effacing bacterial pathogens. *Nat. Med.* **14**, 282–289 (2008).
21. Sonnenberg, G. F., Monticelli, L. A., Elloso, M. M., Fouser, L. A. & Artis, D. CD4<sup>+</sup> lymphoid tissue-inducer cells promote innate immunity in the gut. *Immunity* **34**, 122–134 (2011).
22. Cox, J. H. et al. Opposing consequences of IL-23 signaling mediated by innate and adaptive cells in chemically induced colitis in mice. *Mucosal Immunol.* **5**, 99–109 (2012).

23. Izcue, A. et al. Interleukin-23 restrains regulatory T cell activity to drive T cell-dependent colitis. *Immunity* **28**, 559–570 (2008).
24. Martinez-Barricarte, R. et al. Human IFN- $\gamma$  immunity to mycobacteria is governed by both IL-12 and IL-23. *Sci. Immunol.* **3**, eaau6759 (2018).
25. Mao, K. et al. Innate and adaptive lymphocytes sequentially shape the gut microbiota and lipid metabolism. *Nature* **554**, 255–259 (2018).
26. Sawa, S. et al. ROR $\gamma$ <sup>T</sup> innate lymphoid cells regulate intestinal homeostasis by integrating negative signals from the symbiotic microbiota. *Nat. Immunol.* **12**, 320–326 (2011).
27. Sonnenberg, G. F. & Artis, D. Innate lymphoid cells in the initiation, regulation and resolution of inflammation. *Nat. Med.* **21**, 698–708 (2015).
28. Spits, H. et al. Innate lymphoid cells—a proposal for uniform nomenclature. *Nat. Rev. Immunol.* **13**, 145–149 (2013).
29. Kerdiles, Y. M. et al. Foxo transcription factors control regulatory T cell development and function. *Immunity* **33**, 890–904 (2010).
30. Hossain, D. M. et al. FoxP3 acts as a cotranscription factor with STAT3 in tumor-induced regulatory T cells. *Immunity* **39**, 1057–1069 (2013).
31. Jacobse, J. et al. Interleukin-23 receptor signaling impairs the stability and function of colonic regulatory T cells. *Cell Rep.* **42**, 112128 (2023).
32. Kannan, A. K. et al. IL-23 induces regulatory T cell plasticity with implications for inflammatory skin diseases. *Sci. Rep.* **9**, 17675 (2019).
33. Uhlig, H. H. et al. Differential activity of IL-12 and IL-23 in mucosal and systemic innate immune pathology. *Immunity* **25**, 309–318 (2006).
34. Ahern, P. P. et al. Interleukin-23 drives intestinal inflammation through direct activity on T cells. *Immunity* **33**, 279–288 (2010).
35. Wing, K. et al. CTLA-4 control over Foxp3<sup>+</sup> regulatory T cell function. *Science* **322**, 271–275 (2008).
36. Walker, L. S. & Sansom, D. M. The emerging role of CTLA4 as a cell-extrinsic regulator of T cell responses. *Nat. Rev. Immunol.* **11**, 852–863 (2011).
37. Chang, T. T., Jabs, C., Sobel, R. A., Kuchroo, V. K. & Sharpe, A. H. Studies in B7-deficient mice reveal a critical role for B7 costimulation in both induction and effector phases of experimental autoimmune encephalomyelitis. *J. Exp. Med.* **190**, 733–740 (1999).
38. Lenschow, D. J. et al. CD28/B7 regulation of Th1 and Th2 subsets in the development of autoimmune diabetes. *Immunity* **5**, 285–293 (1996).
39. Tekguc, M., Wing, J. B., Osaki, M., Long, J. & Sakaguchi, S. Treg-expressed CTLA-4 depletes CD80/CD86 by trogocytosis, releasing free PD-L1 on antigen-presenting cells. *Proc. Natl. Acad. Sci. USA* **118**, e2023739118 (2021).
40. Sugiura, D. et al. Restriction of PD-1 function by *cis*-PD-L1/CD80 interactions is required for optimal T cell responses. *Science* **364**, 558–566 (2019).
41. Francisco, L. M. et al. PD-L1 regulates the development, maintenance, and function of induced regulatory T cells. *J. Exp. Med.* **206**, 3015–3029 (2009).
42. Keir, M. E. et al. Tissue expression of PD-L1 mediates peripheral T cell tolerance. *J. Exp. Med.* **203**, 883–895 (2006).
43. Lyu, M. et al. ILC3s select microbiota-specific regulatory T cells to establish tolerance in the gut. *Nature* **610**, 744–751 (2022).
44. Paustian, A. M. S. et al. Continuous IL-23 stimulation drives ILC3 depletion in the upper GI tract and, in combination with TNF $\alpha$ , induces robust activation and a phenotypic switch of ILC3. *PLoS ONE* **12**, e0182841 (2017).
45. Jacquemet, N. et al. Immune checkpoints and innate lymphoid cells—new avenues for cancer immunotherapy. *Cancers (Basel)* **13**, 5967 (2021).
46. Hepworth, M. R. et al. Immune tolerance. Group 3 innate lymphoid cells mediate intestinal selection of commensal bacteria-specific CD4<sup>+</sup> T cells. *Science* **348**, 1031–1035 (2015).
47. Goc, J. et al. Dysregulation of ILC3s unleashes progression and immunotherapy resistance in colon cancer. *Cell* **184**, 5015–5030.e5016 (2021).
48. Klöverpris, H. N. et al. Innate lymphoid cells are depleted irreversibly during acute HIV-1 infection in the absence of viral suppression. *Immunity* **44**, 391–405 (2016).
49. Page, D. B., Postow, M. A., Callahan, M. K., Allison, J. P. & Wolchok, J. D. Immune modulation in cancer with antibodies. *Annu. Rev. Med.* **65**, 185–202 (2014).
50. Lo, B. C. et al. Microbiota-dependent activation of CD4<sup>+</sup> T cells induces CTLA-4 blockade-associated colitis via Fc $\gamma$  receptors. *Science* **383**, 62–70 (2024).

**Publisher's note** Springer Nature remains neutral with regard to jurisdictional claims in published maps and institutional affiliations.

Springer Nature or its licensor (e.g. a society or other partner) holds exclusive rights to this article under a publishing agreement with the author(s) or other rightsholder(s); author self-archiving of the accepted manuscript version of this article is solely governed by the terms of such publishing agreement and applicable law.

© The Author(s), under exclusive licence to Springer Nature Limited 2024

#### JRI Live Cell Bank

David Artis<sup>3</sup>, Randy Longman<sup>3</sup>, Gregory F. Sonnenberg<sup>3</sup>, Ellen Scherl<sup>3</sup>, Robbyn Sockolow<sup>3</sup>, Dana Lukin<sup>3</sup>, Vinita Jacob<sup>3</sup>, Laura Sahyoun<sup>3</sup>, Michael Mintz<sup>3</sup>, Lasha Gogokia<sup>3</sup>, Thomas Ciecierega<sup>3</sup>, Aliza Solomon<sup>3</sup>, Arielle Bergman<sup>3</sup>, Kimberley Chein<sup>3</sup>, Elliott Gordon<sup>3</sup>, Michelle Ramos<sup>3</sup>, Victoria Ribeiro de Godoy<sup>3</sup>, Adriana Bracic-Susak<sup>3</sup>, Sean Oguntunmibi<sup>3</sup>, Dario Garone<sup>3</sup> & Caitlin Mason<sup>3</sup>

# Article

## Methods

### Data reporting

No statistical methods were used to predetermine sample size. The animal experiments were not randomized because littermate group allocation was on the basis of animal genotype; thus, investigators were not blinded to allocation during experiments and data assessment. All experiments were successfully replicated and were independently performed at least two times unless otherwise mentioned.

### Mice

C57BL/6 mice, *Rag1*<sup>-/-</sup> mice<sup>51</sup>, *Il10*<sup>-/-</sup> mice<sup>52</sup> and IL-23R-eGFP mice<sup>53</sup> on a C57BL/6 background were purchased from the Jackson Laboratory and used at 6–12 weeks of age. ROR $\gamma$ <sup>cre</sup> mice<sup>54</sup> on a C57BL/6 background were provided by G. Eberl (Institut Pasteur). C57BL/6 *Ncr1*<sup>cre</sup> mice<sup>55</sup> were provided by E. Vivier and *Ctla4*-floxed mice<sup>56</sup> were provided by S. Sakaguchi. Germ-free mice were maintained at the gnotobiotic facility at Weill Cornell Medicine. Both female and male mice were used in this study. All transgenic mice were bred and maintained in SPF facilities with a 12-h light–dark cycle, an average ambient temperature of 21 °C and an average humidity of 48% at Weill Cornell Medicine. Littermates were used as controls, and sex- and age-matched mice were used in all experiments. In any of these experiments, sex was not found to influence the outcome of the results. No mice were excluded from the analysis unless clearly indicated. All experiments were approved and performed according to the Institutional Animal Care and Use Committee guidelines at Weill Cornell Medicine.

### Isolation of lamina propria immune cells from the intestine of mice

Whole intestines were aseptically removed from the mice and cleaned by removing the fat tissues. For small intestine, Peyer's patches were carefully removed. Afterwards, intestines were opened longitudinally, extensively cleaned with cold Dulbecco's PBS (Corning) and cut approximately into 0.5 cm sections. To dissociate epithelial cells, cut tissues were incubated in Hanks' balanced salt solution containing 5 mM EDTA (Thermo Fisher Scientific), 1 mM dithiothreitol (Sigma-Aldrich) and 2% FBS twice at 37 °C for 20 min. After incubation, the tissues were vortexed; transferred to digestion buffer containing collagenase III (1 mg ml<sup>-1</sup>; Worthington), dispase (0.4 U ml<sup>-1</sup>; Thermo Fisher Scientific), DNase I (20 µg ml<sup>-1</sup>; Sigma-Aldrich) and 10% FBS in RPMI 1640 (Corning); and incubated in a shaker at 200 rpm for 1 h at 37 °C. Leukocytes were enriched by 40%/80% density gradient Percoll centrifugation (GE Healthcare).

### Flow cytometry and cell sorting

Single-cell suspensions were first blocked with anti-CD16/32 antibody (BD Biosciences, 2.4G2) and then incubated with conjugated antibodies in PBS containing 1% FBS and 0.25 mM EDTA on ice. Dead cells were excluded by Fixable Aqua Dead Cell Stain (Thermo Fisher Scientific). The flow cytometry antibodies were purchased from Thermo Fisher Scientific, Biolegend or BD Biosciences. Antibodies targeting TCR $\beta$  (H57-597), B220 (RA3-6B2), CCR6 (29-2L17), CD3 $\epsilon$  (145-2C11), CD4 (RM4-5), CD5 (53-7.3), CD8 $\alpha$  (53-6.7), CD11b (M1/70), CD11c (N418), Ly6G (1AB-Ly6G), CD19 (eBioID3), TCR $\gamma$  $\delta$  (GL3), CD45 (30-F11), CD64 (X54-5/7.1), CD90.2 (30-H12), CD127 (A7R34), F4/80 (BM8), MHCII (MS/114.15.2), NK1.1 (PK136), NKP46 (29A1.4), CD117 (ACK2), CD25 (PC61.5), CD80 (16-10A1), CD86 (GL-1), PD-L1 total (1-111A), PD-L1 free (10F.9G2) and KLRG1 (2F1/KLRG1) were used for surface staining. CTLA-4 (UC10-4B9), FOXP3 (FJK-16S), GATA3 (L50-823), EOMES (Dan11mag), IL-17A (eBio17B7), IL-22 (IL22JOP), IFN $\gamma$  (XMG1.2), Ki67 (Sola15), ROR $\gamma$  (B2D), anti-rabbit IgG (Poly 4064), rat IgG1 isotype control (R3-34) and T-bet (eBio4B10) were used for intracellular staining. Lineage markers for mouse are: CD3 $\epsilon$ , CD5, CD8 $\alpha$ , NK1.1, TCR $\gamma$  $\delta$ , Ly6G, CD11b, CD11c, B220, F4/80. All mouse antibodies were used at 1:200 dilution,

except for CCR6, NKP46 and CTLA-4, which were used at 1:100 dilution. For PD-L1 staining, mouse myeloid cells were first stained with 1-111A anti-PD-L1 monoclonal antibody, to detect total (CD80-bound and free) PD-L1 molecules, and then incubated with 10F.9G2 PD-L1 monoclonal antibody, which competes with CD80 for binding and stain-free PD-L1. The following antibodies were used for cell-surface staining of human samples: CD3 (UCHT1), CD14 (M5E2), CD19 (HIB19), CD34 (581), CD4 (SK3), CD45 (HI30), CD94 (DX22), CD117 (104D2), CD123 (6H6), CD127 (A019D5), Fc $\epsilon$ R1 (AER-37(CRA1), PD-L1 (29E.2A3), CD11c (S-HCL-3), MHCII (L243), CD86 (IT2.2), CD80 (B7-1) and NKP44 (44.189). For free PD-L1 staining, cells were incubated with biotinylated recombinant human PD-1 (CD279)-Fc chimera (Biolegend) followed by PE-Cy5-streptavidin. The following antibodies were used for intracellular staining of human samples: FOXP3 (PCH101), CTLA-4 (14D3), ROR $\gamma$  (Q21-559). All human antibodies were used at 1:100 dilution, except for CD45 and ROR $\gamma$  which were used at 1:50 dilution. Human ILC3s for analysis were gated as CD45<sup>+</sup>CD3<sup>+</sup>CD11c<sup>+</sup>CD14<sup>+</sup>CD19<sup>+</sup>CD34<sup>+</sup>CD94<sup>+</sup>CD123<sup>+</sup>Fc $\epsilon$ R1<sup>+</sup>CD127<sup>+</sup>ROR $\gamma$ <sup>+</sup>. Human myeloid cells were gated as CD45<sup>+</sup>CD3<sup>+</sup>CD4<sup>+</sup>CD11c<sup>+</sup>MHCII<sup>+</sup>. For transcription factors, cells were first stained for surface markers, followed by fixation and permeabilization according to the manufacturer's protocol (FOXP3 staining buffer set from Thermo Fisher Scientific, 00-5123-43). For cytokines, cells were stimulated in RPMI 1640 with 10% FBS, phorbol 12-myristate 13-acetate 50 ng ml<sup>-1</sup> (Sigma-Aldrich), ionomycin 750 ng ml<sup>-1</sup> (Sigma-Aldrich) and brefeldin A 10 µg ml<sup>-1</sup> (Sigma-Aldrich) for 4 h. All flow cytometry experiments were performed on a Fortessa flow cytometer with FACS Diva software (BD Biosciences) and analysed by FlowJo v.10 software. A FACSAria II cell sorter (BD Biosciences) was used for cell sorting.

### Ex vivo stimulation

Sort-purified mouse ILC3s (live, CD45<sup>+</sup>Lin<sup>-</sup>CD90<sup>+</sup>CD127<sup>+</sup>KLRG1<sup>-</sup>CD45<sup>dim</sup>) were cultured in RPMI with high glucose, supplemented with 10% FBS, 10 mM HEPES, 1 mM sodium pyruvate, non-essential amino acids, 80 µM 2-mercaptoethanol, 2 mM glutamine, 100 U ml<sup>-1</sup> penicillin, 100 µg ml<sup>-1</sup> streptomycin (all from Gibco) and Brefeldin A, at 37 °C for 4 h in the presence of recombinant mouse IFN $\gamma$  (20 ng ml<sup>-1</sup>, Biolegend), IL-1 $\beta$  (20 ng ml<sup>-1</sup>, Thermo Fisher Scientific), IL-2 (20 ng ml<sup>-1</sup>, Biolegend), IL-6 (20 ng ml<sup>-1</sup>, Thermo Fisher Scientific), IL-7 (20 ng ml<sup>-1</sup>, Biolegend), IL-12 (20 ng ml<sup>-1</sup>, Thermo Fisher Scientific), IL-15 (20 ng ml<sup>-1</sup>, Biolegend) or IL-23 (20 ng ml<sup>-1</sup>, Biolegend), or in presence or absence of Foxo1 inhibitor (AS1842856, 100 nM) or STAT3 inhibitor (VI-S31-201, 25 µM). The cells were further stained and analysed by flow cytometry. Similarly, immune cells from human tonsil were cultured with recombinant human IL-6 (20 ng ml<sup>-1</sup>, Biolegend), recombinant human IL-2 (20 ng ml<sup>-1</sup>, Biolegend) and recombinant human IL-21 (20 ng ml<sup>-1</sup>, R&D) in presence or absence recombinant human IL-23 (50 ng ml<sup>-1</sup>, Biolegend) with Brefeldin A at 37 °C for 6 h. The cells were further stained and analysed by flow cytometry.

### In vivo administration of antibodies and antibiotics

Anti-IL-23p19 monoclonal antibody (G23-8, BioXCell) was administered intraperitoneally at a dose of 300 µg per mouse every alternate day starting on day 0 and ending on day 5. Anti-NK1.1 monoclonal antibody (PK136, BioXCell) was administered intraperitoneally every 3 d at a dose of 300 µg per mouse starting on day 0 and ending on day 14. A cocktail of antibiotics (0.25 mg ml<sup>-1</sup> of vancomycin, 0.5 mg ml<sup>-1</sup> of ampicillin, neomycin, gentamicin and metronidazole, and 4 mg ml<sup>-1</sup> sucralose) was continuously administered via drinking water for 2 weeks. Mice were regularly monitored for weight change.

### Administration of minicircle vectors

IL-23 and sham minicircle were purchased from System Biosciences. Hydrodynamic injection of 3–6 µg of DNA was carried out in sterile Ringer's solution equivalent to 10% mouse body weight and injected intravenously over 5–7 s.

### **C. rodentium infection**

*C. rodentium* was cultured in LB broth overnight at 37 °C with constant shaking and mice were given oral gavage with 10<sup>9</sup> c.f.u. of bacteria. Faecal pellets were collected at day 5 or 10 after infection and *C. rodentium* c.f.u. were enumerated by plating on MacConkey agar. Mice were euthanized 14 d after infection for analysis. The colon length was measured, and distal colon was used for histological analysis.

### **Adoptive transfer of naive CD4<sup>+</sup> T cells**

Naive CD4<sup>+</sup> T cells were isolated from the spleen and lymph nodes of C57BL/6 mice with an isolation kit following the manufacturer's instructions (Miltenyi Biotech). Recipient mice received 0.5 × 10<sup>6</sup> cells per mouse retro-orbitally. Mice were monitored for weight loss and analysed at the indicated timepoint.

### **Co-culture of intestinal ILC3s and myeloid cells**

Myeloid cells (live, CD45<sup>+</sup>CD90.2<sup>-</sup>CD19<sup>-</sup>B220<sup>-</sup>CD11c<sup>+</sup>MHCII<sup>+</sup>) and ILC3s (live, CD45<sup>+</sup>Lin<sup>-</sup>CD90<sup>-</sup>CD127<sup>-</sup>KLRG1<sup>-</sup>CD45<sup>dim</sup>) were sort-purified from the large intestine of C57BL/6 mice and co-cultured, at the ratio 1:5, at 37 °C with either recombinant IL-23 or heat-killed *C. rodentium* and indicated blocking antibodies. After 6 or 24 h, myeloid cells were first labelled with biotinylated 1-111A anti-PD-L1, then stained with streptavidin, 10F.9G2 anti-PD-L1, anti-CD11c, anti-MHCII, anti-CD80 and anti-CD86 for flow cytometry analysis of CD80, CD86 and PD-L1.

### **Anti-CD40 mouse model colitis**

Indicated mice were treated intraperitoneally with 100 µg of anti-CD40 antibody (IgG2a, monoclonal antibody FGK45 from BioXCell) to induce innate colitis. Mice were analysed and carefully monitored the following week for weight loss.

### **Quantitative PCR**

Sort-purified mouse ILC3s were stimulated with and without IL-23 for 2 h and lysed using RLT plus lysis buffer (Qiagen). RNA was purified using RNeasy Plus Mini Kits (Qiagen) according to the manufacturer's instructions. First-strand complementary DNA was generated using Maxima First Strand cDNA synthesis kit according to the protocol provided by the manufacturer (Thermo Fisher Scientific, K1642). The Power SYBR Green PCR Master Mix (Thermo Fisher Scientific, 4367660) was used for quantitative PCR with ABI7500 (Applied Biosystems). The primer sequences of soluble (s)CTLA-4 and membrane (m)CTLA-4 are as follows: Mouse sCTLA-4: forward: 5'-cgcagattatgtatgtctaaag-3'; reverse: 5'-aacggctttcagtttgatg-3'. Mouse mCTLA-4: forward: 5'-ggcaacggacgcaga-3'; reverse: 5'-ccaaagctaactgcgacaagg-3'. Gene expression was normalized to the internal control *Hprt* for mouse samples.

### **scRNA-seq**

For scRNA-seq, IL-23R<sup>+</sup> immune cells were sorted from small intestine of IL-23R-eGFP mice and stimulated with 30 ng ml<sup>-1</sup> recombinant mouse IL-23 for 2 h. Cells were pooled from three mice. scRNA-seq libraries were generated using the 10X Genomics Chromium system with 3' version 3 chemistry. Libraries were sequenced on an Illumina NovaSeq instrument. Reads were processed by 10X Cell Ranger v.3.1.0 using the mm10 reference genome, resulting in a filtered HDF5 file. scRNA-seq data were further processed and analysed using R v.4.1.2 and the Seurat package v.4.3.0 (ref. 56). Specifically, the Cell Ranger output was imported using the Read10X\_h5 function. Seurat objects were created using only genes that appeared in at least three cells. Cells were further filtered to exclude those with fewer than 1,000 genes detected, more than 5,000 genes detected or more than 10% mitochondrial reads. Read counts were then normalized using the NormalizeData function. The graph representing cells with similar expression patterns was generated with the FindNeighbors function using the 20 largest principal components. A

total of 10,325 unstimulated cells and 8,897 cells with IL-23 stimulation were included in our analyses. Cell clusters were generated using the Louvain algorithm implemented by the FindClusters function with the resolution parameter equal to 0.5. One cluster lacking *Il23r* expression was removed from the analysis and the remaining cells were re-clustered using a resolution of 0.6. Marker genes for each cluster were determined using the Wilcoxon test on the raw counts, implemented by the function FindAllMarkers, and including only positive marker genes with log fold changes greater than 0.25 and Bonferroni-corrected Pvalues less than 0.01. Cluster names were determined by manual inspection of the lists of cluster marker genes. Dimensionality reduction by UMAP was performed using the RunUMAP function with the 20 largest principal components. All visualizations of scRNA-seq data were generated using the Seurat package, as well as ggplot2 v.3.3.3.

### **Human sample collection**

Human tonsil and surgical resection samples from patients with IBD were provided by the Cooperative Human Tissue Network (CHTN), which is funded by the National Cancer Institute. Other investigators may have received specimens from the same patients. Samples were received as entirely de-identified human specimens with diagnoses confirmed by medical records and trained pathologists. This protocol was reviewed by the Weill Cornell Medicine institutional review board and determined to meet the exemption category 4 of HHS 45 CFR 46.104(d). Further oversight of the CHTN is outlined at www.chtn.org. Intestinal biopsies from the colon of individuals with Crohn's disease and sex- and age-matched controls without IBD were obtained following Institutional Review Board-approved protocols from the JRI Live Cell Bank Consortium at Weill Cornell Medicine (protocol number 1503015958). Informed consent was obtained from all subjects. Biopsies were cryopreserved in 90% FBS and 10% dimethylsulfoxide for future side-by-side comparison.

### **Human tissue processing and isolation of ILC3s**

Human surgical intestinal samples were incubated with continuous shaking in PBS containing 5% FBS, 1 mM EDTA and 1 mM dithiothreitol for 30 min at 37 °C to remove the epithelial cells. After incubation, the tissues were vortexed, and similarly transferred to digestion buffer containing 2 mg ml<sup>-1</sup> Collagenase D (Sigma) and 0.1 µg ml<sup>-1</sup> DNase I (Sigma) in RPMI 1640 (Corning) with 5% FBS for 1 h. After digestion, the single-cell suspension was passed through a 70 µM cell strainer to obtain the cells. Furthermore, the cells were immediately cryopreserved for future use. For sorting of human ILC3s, frozen samples were thawed, washed once in RPMI with 5% FBS, treated with Fc receptor block (BD Biosciences, 2.4G2) for 10 min and surface stained. ILC3s were sorted as live CD45<sup>+</sup>Lineage<sup>-</sup> (CD3e, CD34, CD19, CD94, CD14, CD123, FcεRIα, CD11c) CD127<sup>+</sup>, CRTH2<sup>-</sup>, CD117<sup>+</sup> cells. Tonsil samples were dissociated mechanically by a syringe plunger and cells were filtered through a 70 µM cell strainer and cryopreserved in 90% FBS and 10% dimethylsulfoxide for a future side-by-side comparison. Following thawing, cells were used directly for staining. Intestinal biopsies were immediately cryopreserved in 90% FBS and 10% dimethylsulfoxide for future side-by-side comparison. Following thawing, tissues were incubated in 0.5 mg ml<sup>-1</sup> collagenase D and 20 mg ml<sup>-1</sup> DNase I for 1 h at 37 °C with shaking. After digestion, remaining tissues were further dissociated mechanically by a syringe plunger. Cells were filtered through a 70 µM cell strainer and used directly for staining.

### **Bulk RNA sequencing**

ILC3s gated as live CD45<sup>+</sup>Lineage<sup>-</sup> (CD3e, CD34, CD19, CD94, CD14, CD123, FcεRIα, CD11c) CD127<sup>+</sup>, CRTH2<sup>-</sup>, CD117<sup>+</sup> were sorted from the inflamed and matched adjacent non-inflamed intestine that was resected from patients with IBD, encompassing both Crohn's disease and ulcerative colitis. These cells were used to prepare RNA sequencing libraries by the Epigenomics Core at Weill Cornell Medicine, using the Clontech

# Article

SMARTer Ultra Low Input RNA Kit V4 (Clontech Laboratories). Sequencing was performed on an Illumina HiSeq 4000, yielding 50-base-pair single-end reads. Raw sequencing reads were demultiplexed with Illumina CASAVA (v.1.8.2). Adaptors were trimmed from reads using FLEXBAR (v.2.4) and reads were aligned to the NCBI GRCh37/hg19 human genome using the STAR aligner (v.2.3.0) with default settings. Reads per gene were counted using Rsubread. Before differential expression analysis, genes were prefiltered, keeping only those genes with 50 or more counts in at least two samples. Differential expression analysis was performed using DESeq2 (v.1.20.0) using both site (inflamed/adjacent) and patient ID as factors in the design. A false discovery rate of 0.1 was taken to indicate significance. The volcano plot was generated using dplyr (v.1.1.3), ggplot2 (v.3.4.3) and ggrepel (v.0.9.3) in R (v.4.1.2).

## Histological staining and blinded histopathological scoring

Large intestinal Swiss rolls were fixed in 4% paraformaldehyde and embedded in paraffin. Five-micrometre sections were stained with H&E. Images were taken using a Nikon Eclipse Ti microscope and NIS-Elements 4.30.02 software (Nikon). Histological scoring of H&E-stained tissues was done following these parameters. Each mouse was scored in a blinded manner on a grade of 0–4 (0 = none; 4 = most severe) for the following four pathological parameters for a maximum score of 16: (1) inflammatory cell infiltration; (2) goblet-cell depletion; (3) mucosa thickening/oedema; and (4) destruction of crypt architecture.

## Statistical analysis

All statistical analyses were performed by GraphPad Prism v.9 software. Mann–Whitney *U*-test or one-way ANOVA with 95% confidence interval followed by Dunnett's multiple comparisons was used to determine the *P* values for the datasets. Correlative analyses were compared by non-parametric Spearman correlation. *P* values smaller than 0.05 were considered significant.

## Reporting summary

Further information on research design is available in the Nature Portfolio Reporting Summary linked to this article.

## Data availability

All data necessary to understand and evaluate the conclusions of this paper are provided. Single-cell RNA sequencing data have been

deposited in the Gene Expression Omnibus database under the accession number GSE229976. Bulk RNA sequencing data have been deposited under the accession number GSE247742. Source data are provided with this paper.

51. Mombaerts, P. et al. RAG-1-deficient mice have no mature B and T lymphocytes. *Cell* **68**, 869–877 (1992).
52. Kühn, R., Löhler, J., Rennick, D., Rajewsky, K. & Müller, W. Interleukin-10-deficient mice develop chronic enterocolitis. *Cell* **75**, 263–274 (1993).
53. Awasthi, A. et al. Cutting edge: IL-23 receptor gfp reporter mice reveal distinct populations of IL-17-producing cells. *J. Immunol.* **182**, 5904–5908 (2009).
54. Lochner, M. et al. In vivo equilibrium of proinflammatory IL-17<sup>+</sup> and regulatory IL-10<sup>+</sup> Foxp3<sup>+</sup> ROR $\gamma$ T cells. *J. Exp. Med.* **205**, 1381–1393 (2008).
55. Narni-Mancinelli, E. et al. Fate mapping analysis of lymphoid cells expressing the NKp46 cell surface receptor. *Proc. Natl Acad. Sci. USA* **108**, 18324–18329 (2011).
56. Butler, A., Hoffman, P., Smibert, P., Papalexi, E. & Satija, R. Integrating single-cell transcriptomic data across different conditions, technologies, and species. *Nat. Biotechnol.* **36**, 411–420 (2018).

**Acknowledgements** We thank members of the Sonnenberg Laboratory for discussions and critical reading of the manuscript. Research in the Sonnenberg Laboratory is supported by the US National Institutes of Health (grant nos. R01AI143842, R01AI123368, R01AI145989, U01AI095608, R01AI162936, R01CA274534 and R37AI174468), an Investigators in the Pathogenesis of Infectious Disease Award from the Burroughs Wellcome Fund, the Meyer Cancer Center Collaborative Research Initiative, the Dalton Family Foundation and Linda and Glenn Greenberg. A.A. and M.L. are supported by fellowships from the Crohn's and Colitis Foundation (grant nos. 902451 and 935259). A.M.J. and J.U. are supported by US National Institutes of Health grant no. T32DK116970. J.Z. is supported by grant no. F32DK136248. V.H. is supported by a DFG Walter Benjamin Fellowship (grant no. HO 7399/1-1). G.F.S. is a CRI Lloyd J. Old STAR. We thank the Epigenomics Cores of Weill Cornell Medicine, N. Zahan for administrative support and D. Garone and A. Brcic-Susak for technical support. The Jill Roberts Institute (JRI) Live Cell Bank is supported by the JRI, the Jill Roberts Center for IBD, Cure for IBD, the Rosanne H. Silbermann Foundation, the Sanders Family and Weill Cornell Medicine Division of Pediatric Gastroenterology and Nutrition.

**Author contributions** A.A. and G.F.S. conceived the project. A.A. performed most experiments and analysed the data. A.M.J., J.Z., V.H., J.U., M.L. and J.G. helped with experiments and data analyses. JRI Live Cell Bank and R.E.S. contributed to clinical sample acquisition, annotation, processing and evaluation. J.B.W., E.V. and S.S. provided essential mouse models, scientific advice and expertise. A.A. and G.F.S. wrote the manuscript, with input from all of the authors.

**Competing interests** The authors declare no competing interests.

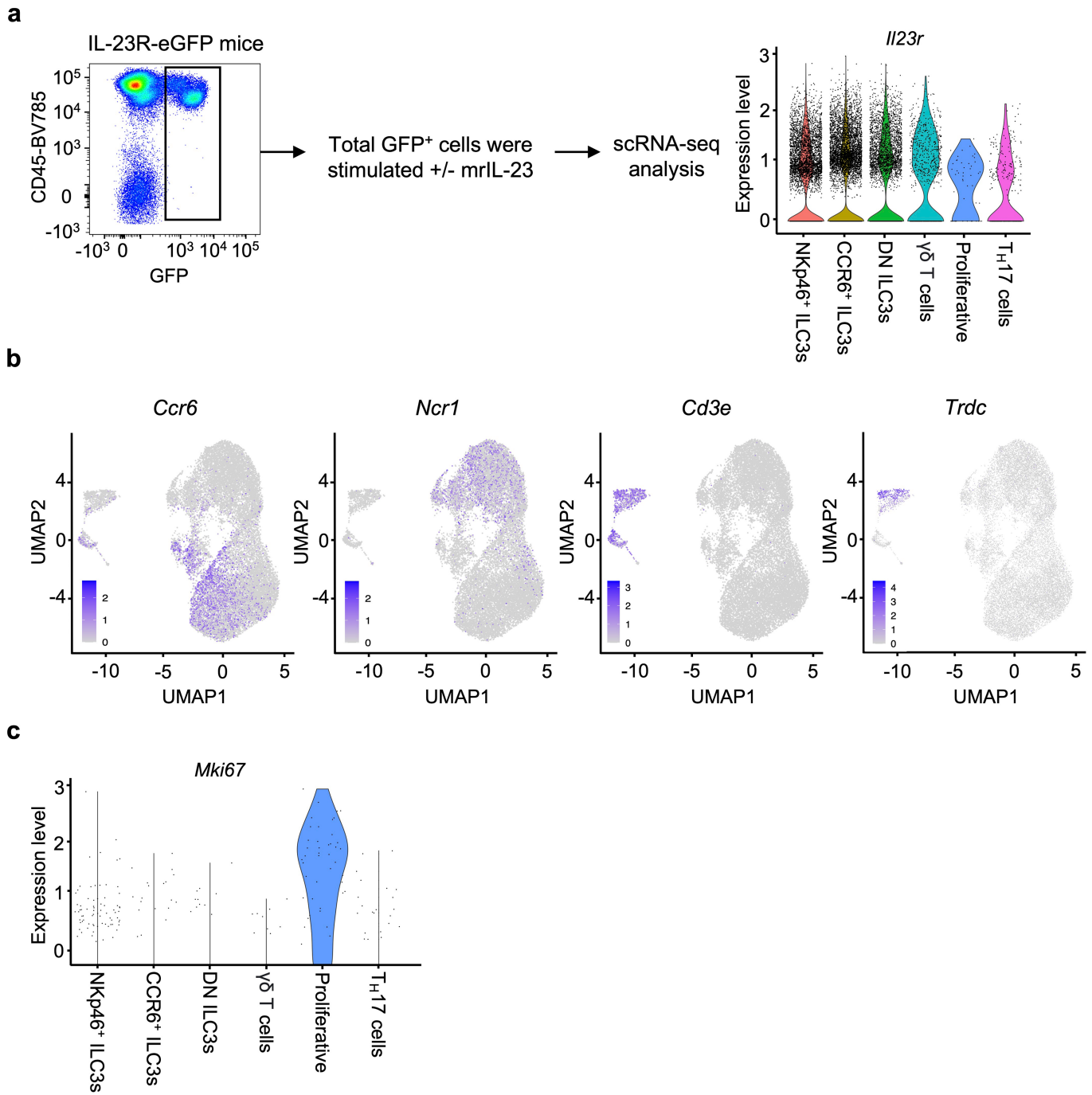
### Additional information

**Supplementary information** The online version contains supplementary material available at <https://doi.org/10.1038/s41586-024-07537-3>.

**Correspondence and requests for materials** should be addressed to Gregory F. Sonnenberg.

**Peer review information** *Nature* thanks the anonymous reviewers for their contribution to the peer review of this work.

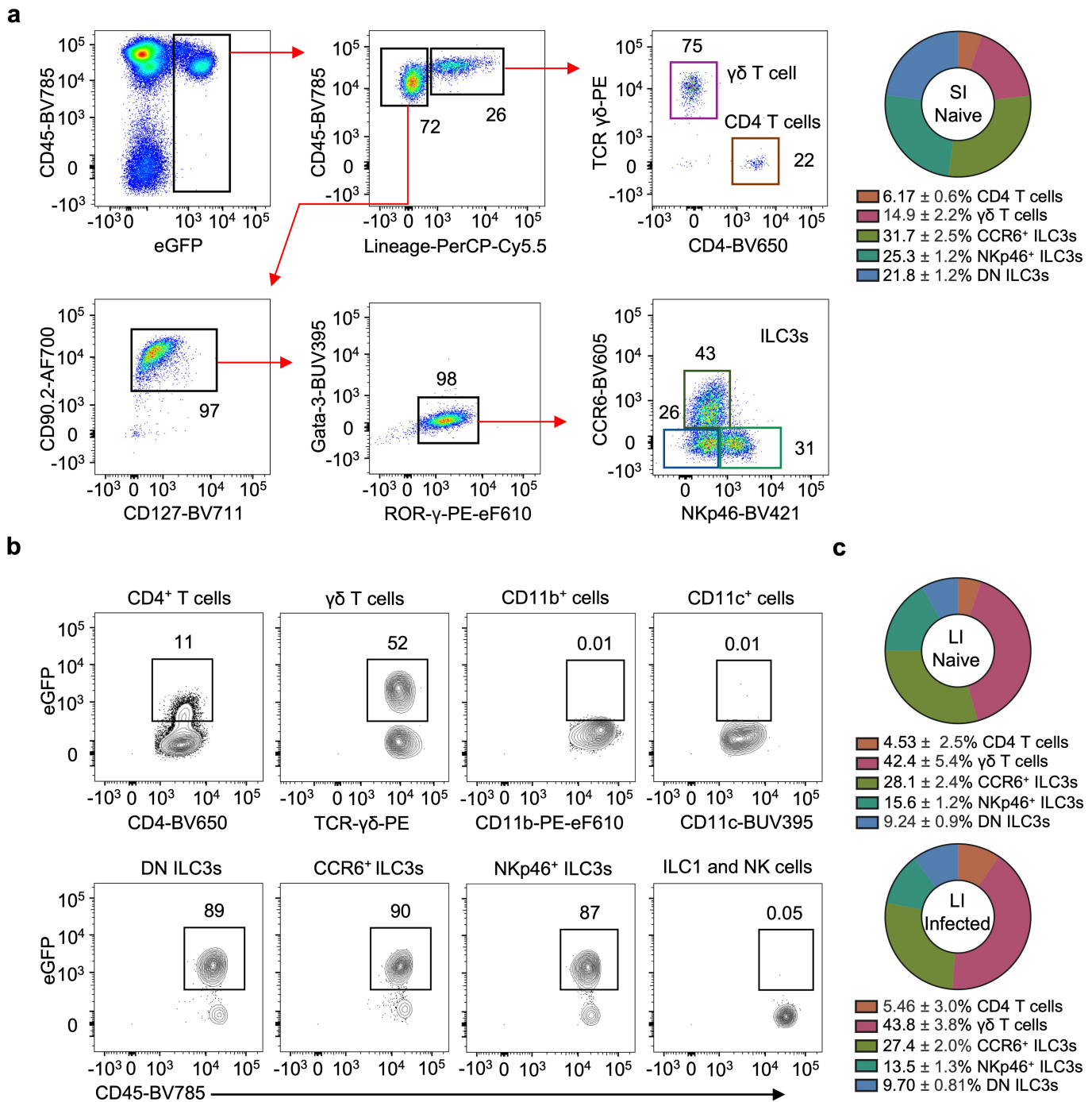
**Reprints and permissions information** is available at <http://www.nature.com/reprints>.



**Extended Data Fig. 1 | Single cell analysis of all IL-23R<sup>+</sup> cells in small intestine of healthy mice.** **a**, Gating strategy and experimental design to sort IL-23R<sup>+</sup> immune cells from small intestine lamina propria of IL-23R-eGFP mice for scRNA-seq. Violin plot confirming *IL23r* expression among all the identified

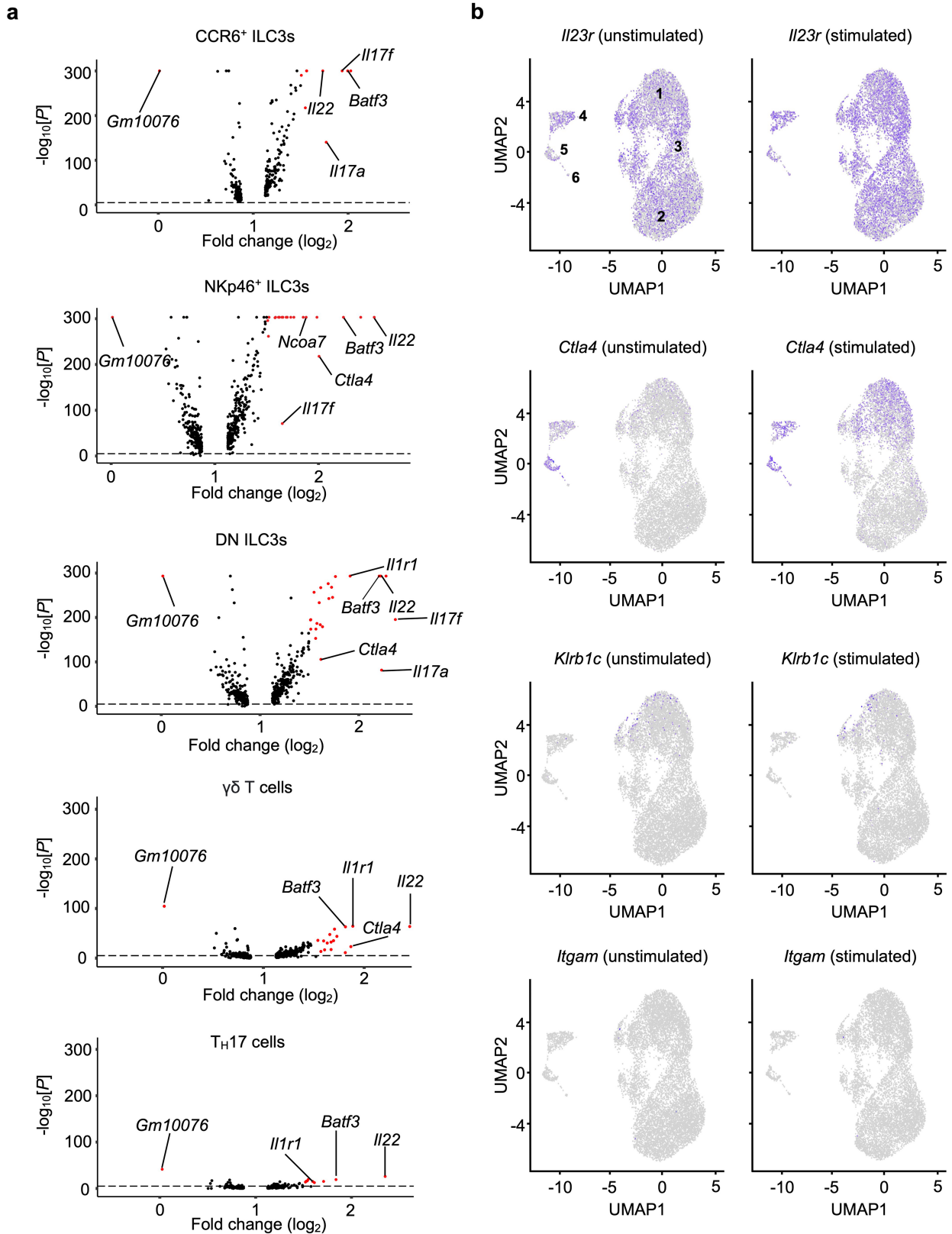
IL-23R<sup>+</sup> cell clusters. **b**, Feature plots showing expression of indicated genes in different clusters. **c**, Violin plot showing *Mki67* expression among all identified IL-23R<sup>+</sup> cell clusters.

# Article



**Extended Data Fig. 2 | Characterization of IL-23R<sup>+</sup> immune cells in the intestine.** **a.**, Flow cytometry plots with donut plot of final frequencies of different IL-23R<sup>+</sup> immune cells in small intestine lamina propria of IL-23R-eGFP mice ( $n = 4$  mice). Lineage 1, CD11b, CD11c, B220, CD3e, CD5, CD8α, NK1.1 and TCRγδ. **b.**, Flow cytometry plots showing eGFP expression (IL-23R) in different

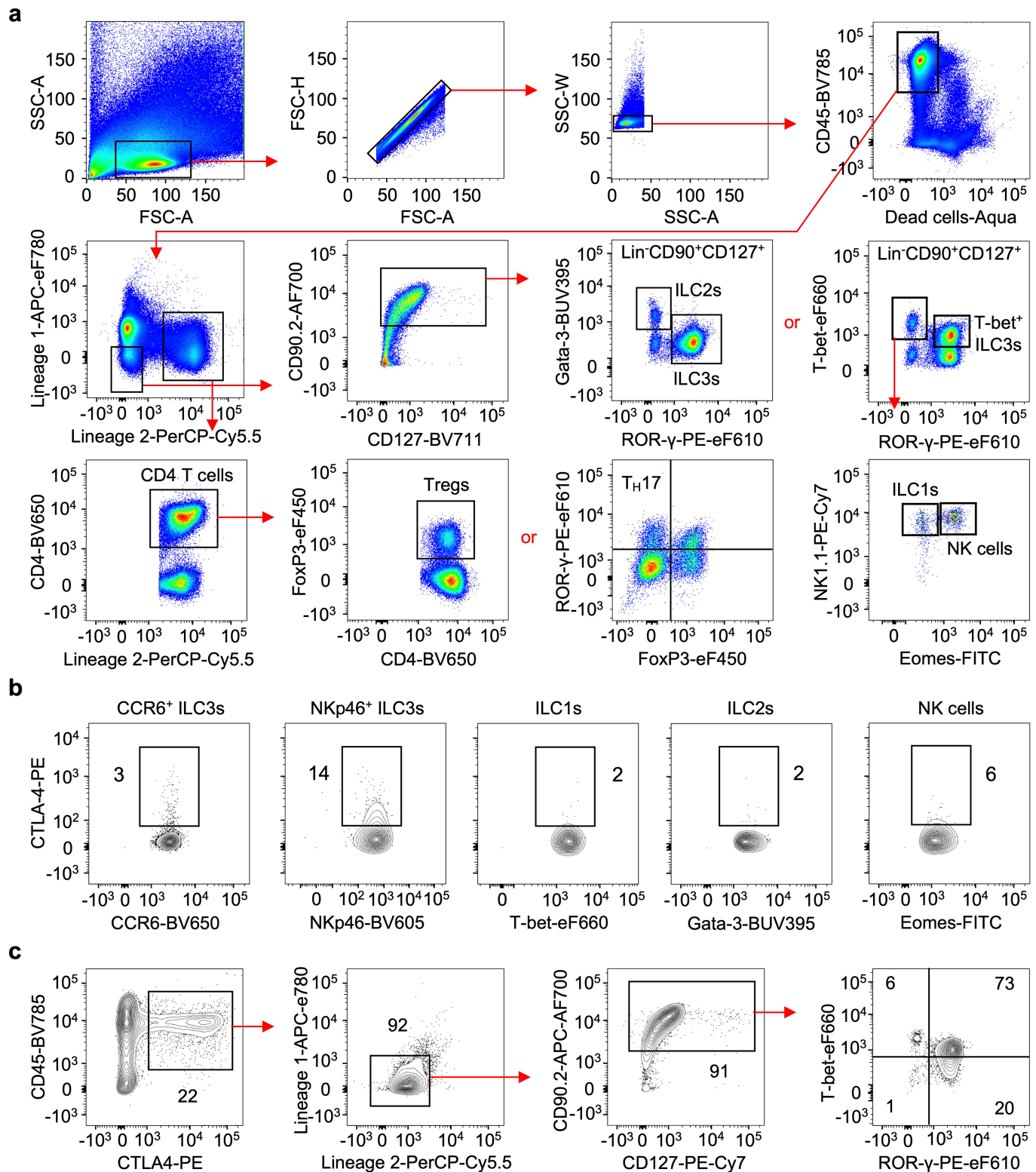
immune cells in small intestine lamina propria of IL-23R-eGFP mice ( $n = 4$  mice). **c.**, Donut plots of final frequencies of different IL-23R<sup>+</sup> immune cells in large intestine lamina propria of naïve and *C. rodentium* infected IL-23R-eGFP mice at day 14 post infection ( $n = 4$  mice). Data in **a** and **c** are representative of two or three independent experiments with similar results.



**Extended Data Fig. 3 | Acute IL-23 driven responses in IL-23R<sup>+</sup> intestinal cells.** **a**, Volcano plots of differentially expressed genes in scRNA-seq dataset from IL-23R<sup>+</sup> immune cells from the small intestine of IL-23R-eGFP mice before and after IL-23 stimulation in annotated cell types. **b**, UMAP plots of scRNA-seq

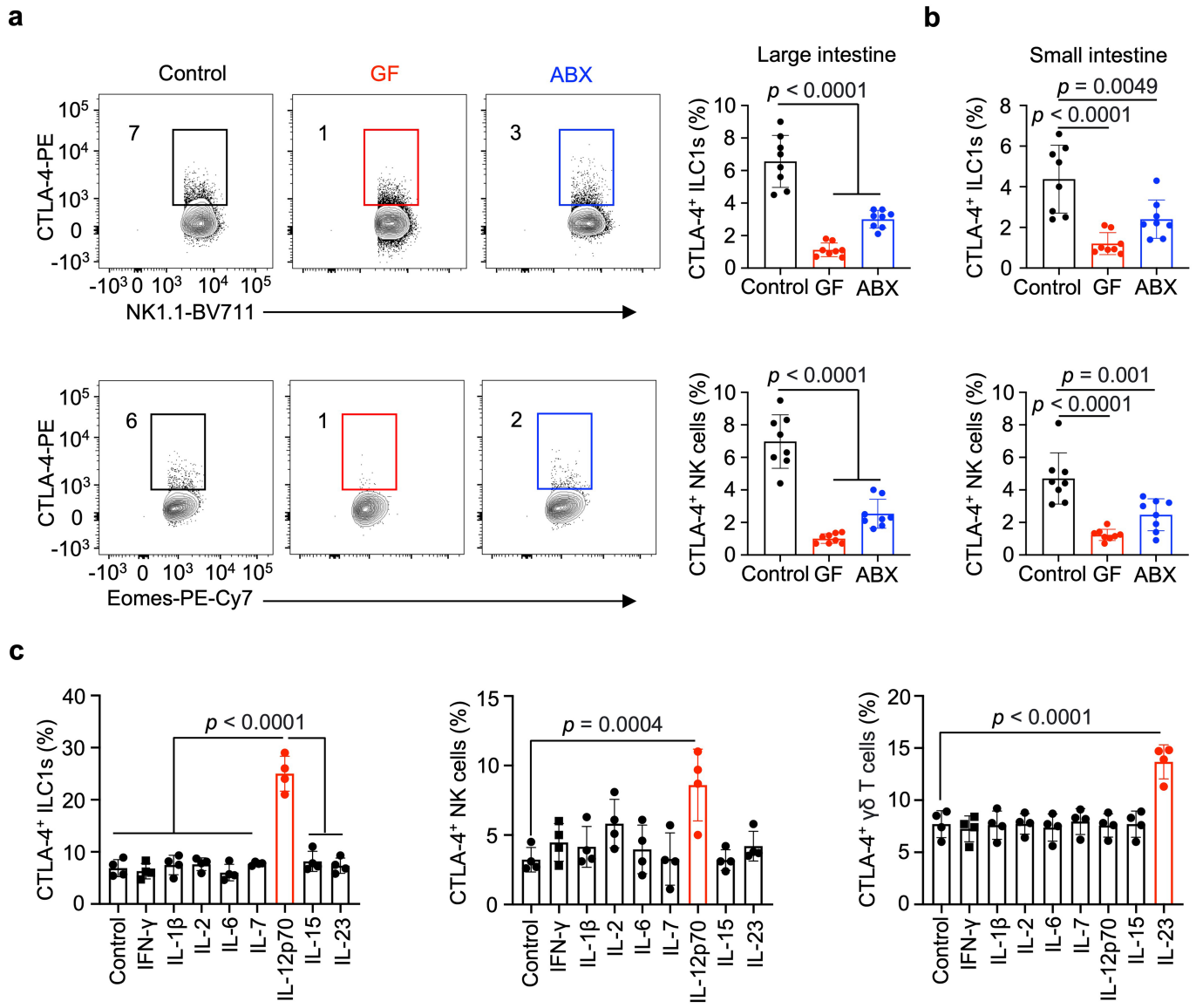
data showing indicated gene expression in different clusters before and after IL-23 stimulation (1-NKp46<sup>+</sup> ILC3s, 2-CCR6<sup>+</sup> ILC3s, 3-DN ILC3s, 4- $\gamma\delta$  T cells, 5- $T_{H17}$  cells, 6-Proliferative cells). The statistics was obtained by the Wilcoxon test as implemented by Seurat; red dots are significantly different.

# Article



**Extended Data Fig. 4 | Flow cytometry gating for ILCs and CTLA-4.** **a.**, Gating strategy for flow cytometry analysis of different immune cells in intestinal lamina propria of mice. Lineage 1, CD11b, CD11c, F4/80 and B220; lineage 2, CD3 $\epsilon$ , CD5, CD8 $\alpha$  and TCR $\gamma\delta$ ; Group 1 innate lymphoid cells (ILC1s) were identified as live CD45 $^+$  Lineage $^-$  CD127 $^+$  CD90.2 $^+$  T-bet $^+$  ROR $\gamma^-$  NK1.1 $^+$  Eomes $^-$ ; group 2 innate lymphoid cells (ILC2s) were identified as live CD45 $^+$  Lineage $^-$  CD127 $^+$  CD90.2 $^+$  GATA3 $^+$ ; group 3 innate lymphoid cells (ILC3s) were identified as live CD45 $^+$  Lineage $^-$  CD127 $^+$  CD90.2 $^+$  ROR $\gamma^+$ ; and subsets of ILC3s were further

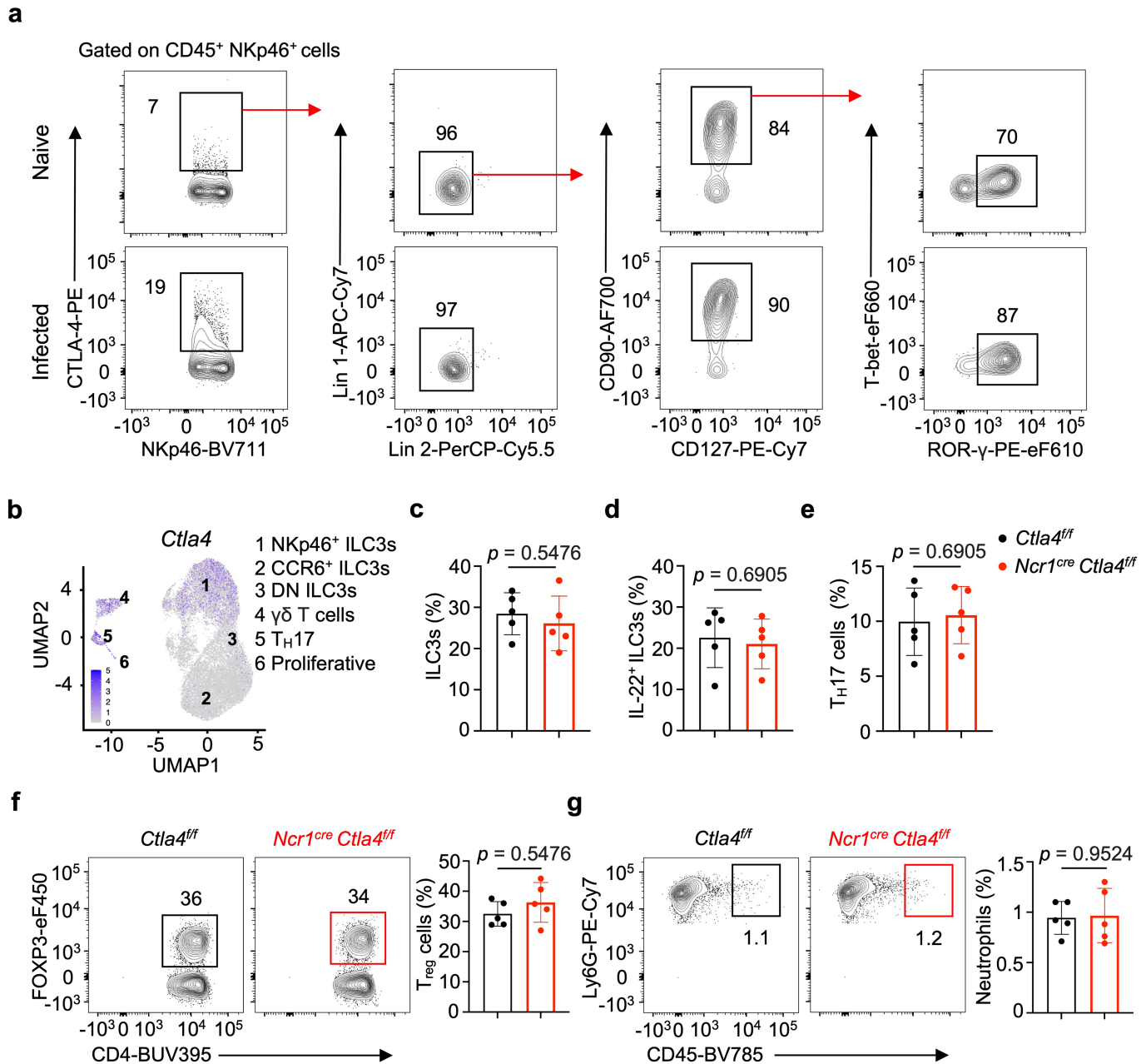
identified as CCR6 $^+$  T-bet $^+$  ILC3s or CCR6 $^-$  T-bet $^+$  ILC3s. For T cell analysis Tregs were identified as CD45 $^+$  CD4 $^+$  FoxP3 $^+$  T cells and  $T_{H17}$  as CD45 $^+$  CD4 $^+$  ROR $\gamma$  $^+$  FoxP3 $^+$  T cells. **b.**, Representative flow cytometry plots of CTLA-4 staining in different immune cells from small intestine lamina propria of C57BL/6 mice ( $n = 4$  mice). **c.**, Flow cytometry plots of CTLA-4 $^+$  cells in small intestine lamina propria of  $Rag1^{-/-}$  mice ( $n = 4$  mice). Data in **b** and **c** are representative of two independent experiments with similar results.



**Extended Data Fig. 5 | Microbiota dependent regulation of CTLA-4.** **a**, Flow cytometry plots with graph of CTLA-4<sup>+</sup> ILC1s and CTLA-4<sup>+</sup> NK cells frequencies in large intestine lamina propria of conventional SPF, germ-free (GF) and SPF *Rag1*<sup>-/-</sup> mice treated with antibiotics (ABX) (n = 8 mice). **b**, Graph of CTLA-4<sup>+</sup> ILC1s and CTLA-4<sup>+</sup> NK cells frequencies in small intestine lamina propria of conventional SPF, germ-free and SPF mice treated with antibiotics on *Rag1*<sup>-/-</sup> background (n = 8 mice). **c**, Graph of CTLA-4<sup>+</sup> ILC1s, CTLA-4<sup>+</sup> NK cells and

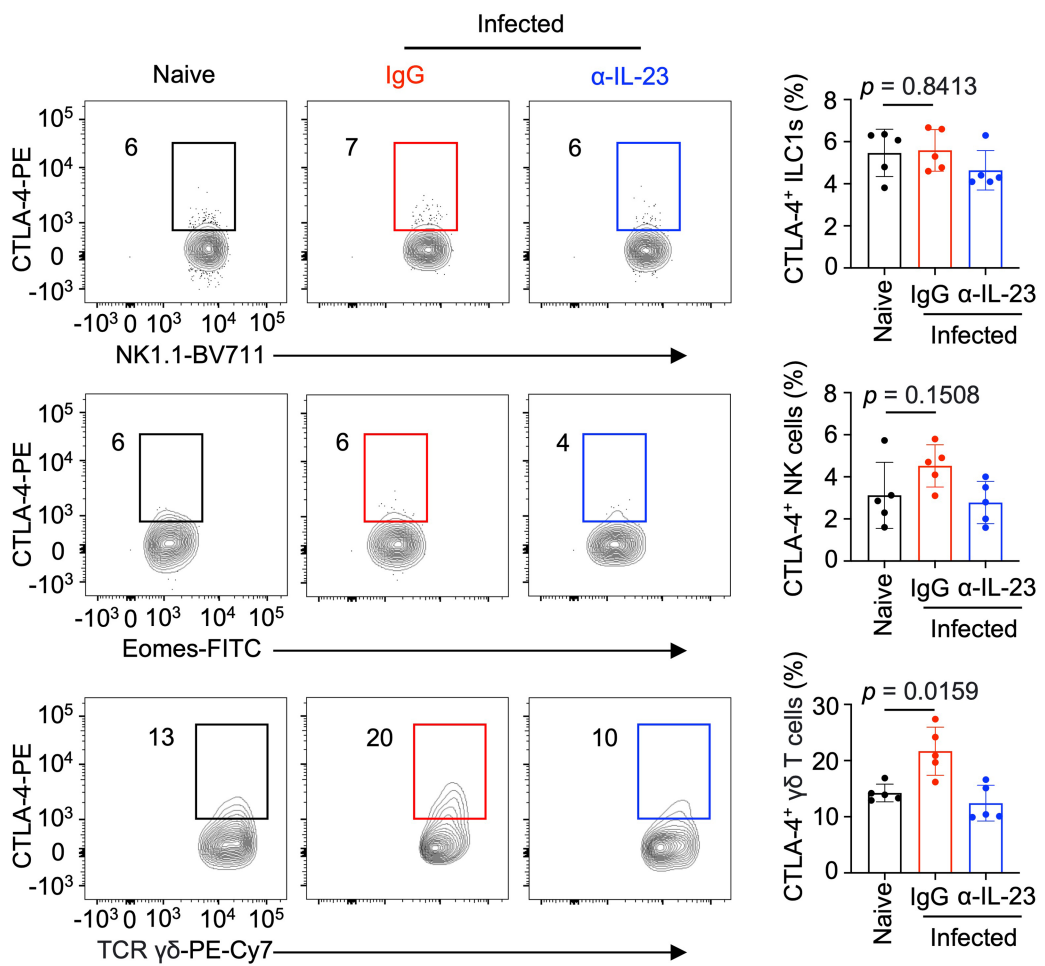
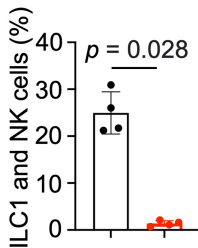
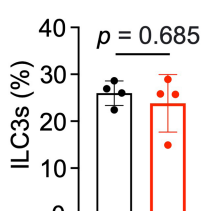
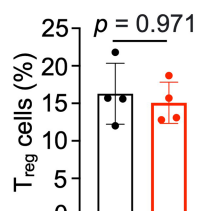
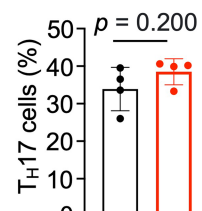
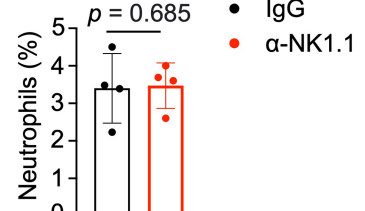
CTLA-4<sup>+</sup> γδ T cells frequencies in small intestine lamina propria of SPF mice ex vivo stimulated with indicated cytokines (n = 4 mice). Data in **a–b** were pooled from two independent experiments and shown as Mean ± s.d. Data in **c** are representative of two or three independent experiments with similar results and shown as Mean ± s.d. The statistics in **a–c** were calculated by one-way ANOVA with Dunnett's multiple comparisons.

# Article



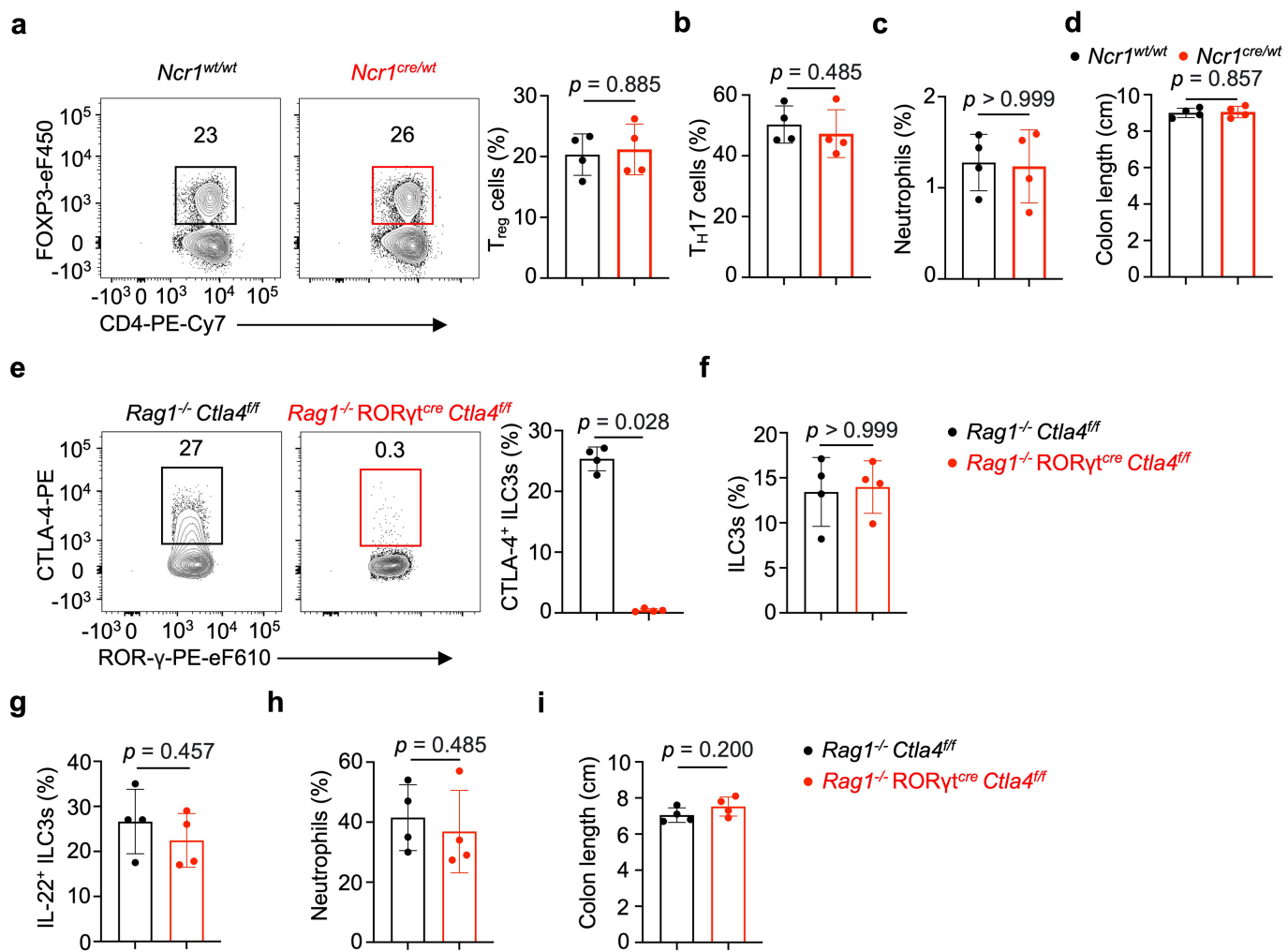
**Extended Data Fig. 6 | Steady state analysis of *Ncr1<sup>cre</sup> Ctla4<sup>ff</sup>* mice.** **a**, Flow cytometry plots of NKp46<sup>+</sup> cells in large intestine lamina propria of naïve and *C. rodentium* infected C57BL/6 mice ( $n = 4$  mice). Lineage 1, CD11b, CD11c and B220; lineage 2, CD3 $\epsilon$ , CD5, CD8 $\alpha$ , and TCR $\gamma\delta$ . **b**, UMAP plot of scRNA-seq data of IL-23R<sup>+</sup> immune cells from the small intestine of IL-23R-eGFP mice showing *Ctla4* expression in different clusters. The large intestine of *Ncr1<sup>cre</sup> Ctla4<sup>ff</sup>* and *Ctla4<sup>ff</sup>* were analyzed at steady state and graph displaying the frequency of **(c)** ILC3s (percentage of Lin<sup>+</sup> CD90<sup>+</sup> CD127<sup>+</sup>) and **(d)** IL-22<sup>+</sup> ILC3s (percentage of

total ILC3s). **e**, Graph of T<sub>H</sub>17 cells frequency (percentage of CD4<sup>+</sup> T cells). Flow plots with graph displaying the frequency of **(f)** Treg cells (percentage of CD4<sup>+</sup> T cells) and **(g)** neutrophils gated as CD11b<sup>+</sup> Ly6G<sup>+</sup> cells (percentage of CD45<sup>+</sup> cells). Data in **a,c,d,e,f** and **g** are representative of two or three independent experiments with similar results ( $n = 5$  mice) and shown as Mean  $\pm$  s.d. The statistics in **c-g** were determined by Mann-Whitney *U*-test (unpaired, two-tailed).

**a****b****c****d****e****f**

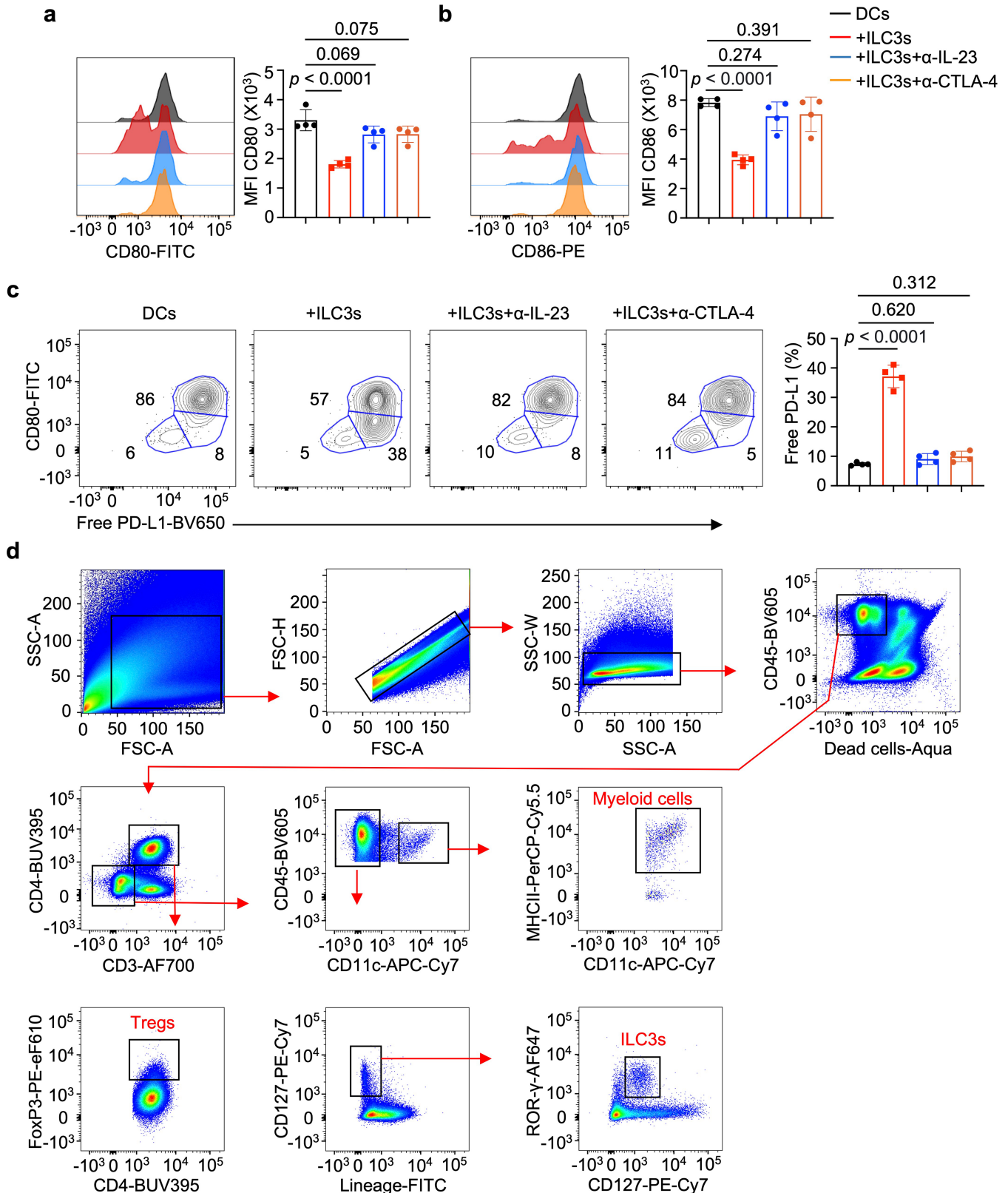
**Extended Data Fig. 7 | NK cells and ILCs do not impact intestinal inflammation following enteric infection with *C. rodentium*.** C57BL/6 mice were orally infected with *C. rodentium* and treated with IgG or anti-IL-23 monoclonal antibody. **a**, Flow cytometry plots with graph displaying the frequency of CTLA-4 expression on ILC1s, NK cells and  $\gamma\delta$  T cells ( $n = 5$  mice). C57BL/6 mice were orally infected with *C. rodentium* and treated with IgG or anti-NK1.1 monoclonal antibody. Mice were analyzed at day 14 post infection and graph displaying the **(b)** depletion efficiency of natural killer cells and

ILCs, and the frequency of **(c)** ILC3s (percentage of Lin<sup>-</sup> CD90<sup>+</sup> CD127<sup>+</sup>); **(d)** Treg cells (percentage of CD4<sup>+</sup> T cells); **(e)** T<sub>H</sub>17 cells (percentage of CD4<sup>+</sup> T cells); **(f)** Neutrophils gated as CD11b<sup>+</sup> Ly6G<sup>+</sup> cells (percentage of CD45<sup>+</sup> cells) in large intestinal lamina propria immune cells. Data in **b-f** are representative of two or three independent experiments with similar results ( $n = 4$  mice) and shown as Mean  $\pm$  s.d. The statistics in **a-f** were determined by Mann-Whitney U-test (unpaired, two-tailed).



**Extended Data Fig. 8 | Innate immune responses are intact in mice lacking ILC3-specific CTLA-4.** *Ncr1<sup>wt/wt</sup>* and *Ncr1<sup>cre/wt</sup>* mice were orally infected with *C. rodentium* and at day 14 post infection large intestinal lamina propria immune cells were analyzed. **a**, Flow cytometry plots with graph of Tregs frequency (percentage of CD4<sup>+</sup> T cells) and graph displaying the frequency of (**b**) T<sub>H17</sub> cells (percentage of CD4<sup>+</sup> T cells) and (**c**) neutrophils gated as CD11b<sup>+</sup>Ly6G<sup>+</sup> cells (percentage of CD45<sup>+</sup> cells) with (**d**) colon length. **e**, Flow cytometry plots and graph of CTLA-4<sup>+</sup> ILC3s frequency (percentage of total ILC3s) in *Rag1<sup>-/-</sup> Ctla4<sup>ff</sup>*

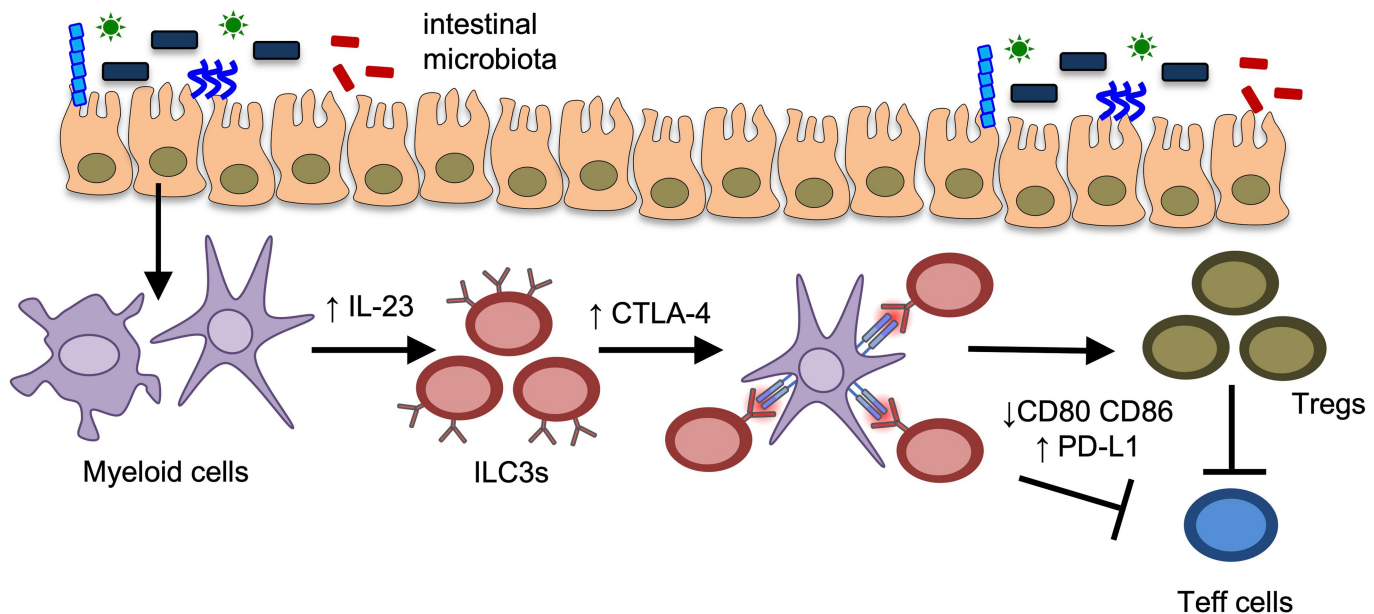
and *Rag1<sup>-/-</sup> RORyt<sup>cre</sup> Ctla4<sup>ff</sup>* mice. *Rag1<sup>-/-</sup> Ctla4<sup>ff</sup>* and *Rag1<sup>-/-</sup> RORyt<sup>cre</sup> Ctla4<sup>ff</sup>* mice were treated with 100 µg of anti-CD40 antibody, and graph displaying the frequency of (**f**) ILC3s (percentage of Lin<sup>-</sup> CD90<sup>+</sup> CD127<sup>+</sup>); (**g**) IL-22<sup>+</sup> ILC3s (percentage of total ILC3s) and (**h**) neutrophils gated as CD11b<sup>+</sup>Ly6G<sup>+</sup> cells (percentage of CD45<sup>+</sup> cells) in the large intestines with (**i**) colon length at day 7 post treatment. Data in **a-i** are representative of two independent experiments with similar results (*n* = 4 mice) and shown as Mean ± s.d. The statistics in **a-i** were determined by Mann-Whitney *U*-test (unpaired, two-tailed).



**Extended Data Fig. 9 | CTLA-4<sup>+</sup> ILC3s reduce co-stimulatory molecules and enhance PD-L1 on myeloid cells in response to IL-23.** Sorted ILC3s and myeloid cells from the large intestine of C57BL/6 mice were co-cultured with recombinant IL-23 in presence or absence of indicated blocking antibodies. Flow cytometry plots with graph of MFI of (a) CD80 and (b) CD86 expression on myeloid cells gated as CD11c<sup>+</sup> MHCII<sup>hi</sup>. c, Flow cytometry plots with graph of

free PD-L1 frequency on myeloid cells gated as CD11c<sup>+</sup> MHCII<sup>hi</sup>. d, Gating strategy to analyze T cells, myeloid cells and ILC3s in human samples. Data in a-c are representative of two independent experiments with similar results ( $n = 4$  mice) and shown as Mean  $\pm$  s.d. The statistics were calculated by one-way ANOVA with Dunnett's multiple comparisons.

## Article



### Extended Data Fig. 10 | ILC3s restrain IL-23 mediated inflammation

**through CTLA-4.** Here we define a pathway of immune regulation in the large intestine. This pathway is activated by gut microbes and IL-23 in a FOXO1- and STAT3-dependent manner. ILC3-intrinsic CTLA-4 shapes the levels of co-inhibitory and co-stimulatory molecules on intestinal myeloid cells to

support Tregs and restrict T effector (Teff) cells. Consequently, ILC3-intrinsic CTLA-4 function as a checkpoint to restrain the pathologic functions of IL-23, suggesting that disruption of these lymphocytes, which occurs in IBD, contributes to chronic inflammation.

Corresponding author(s): Gregory F. Sonnenberg

Last updated by author(s): 04/25/2024

## Reporting Summary

Nature Portfolio wishes to improve the reproducibility of the work that we publish. This form provides structure for consistency and transparency in reporting. For further information on Nature Portfolio policies, see our [Editorial Policies](#) and the [Editorial Policy Checklist](#).

### Statistics

For all statistical analyses, confirm that the following items are present in the figure legend, table legend, main text, or Methods section.

n/a Confirmed

- The exact sample size ( $n$ ) for each experimental group/condition, given as a discrete number and unit of measurement
- A statement on whether measurements were taken from distinct samples or whether the same sample was measured repeatedly
- The statistical test(s) used AND whether they are one- or two-sided  
*Only common tests should be described solely by name; describe more complex techniques in the Methods section.*
- A description of all covariates tested
- A description of any assumptions or corrections, such as tests of normality and adjustment for multiple comparisons
- A full description of the statistical parameters including central tendency (e.g. means) or other basic estimates (e.g. regression coefficient) AND variation (e.g. standard deviation) or associated estimates of uncertainty (e.g. confidence intervals)
- For null hypothesis testing, the test statistic (e.g.  $F$ ,  $t$ ,  $r$ ) with confidence intervals, effect sizes, degrees of freedom and  $P$  value noted  
*Give  $P$  values as exact values whenever suitable.*
- For Bayesian analysis, information on the choice of priors and Markov chain Monte Carlo settings
- For hierarchical and complex designs, identification of the appropriate level for tests and full reporting of outcomes
- Estimates of effect sizes (e.g. Cohen's  $d$ , Pearson's  $r$ ), indicating how they were calculated

*Our web collection on [statistics for biologists](#) contains articles on many of the points above.*

### Software and code

Policy information about [availability of computer code](#)

#### Data collection

All flow cytometry experiments were performed using an LSR Fortessa flow cytometer and the FACS Diva software v9.0 (BD Biosciences) or sort-purified by using FACSAria II cell sorter (BD Biosciences). Single-cell RNA sequencing (scRNA-seq) libraries were generated using the 10X Genomics Chromium system with 3' version 3 chemistry. Libraries were sequenced on an Illumina NovaSeq instrument. Reads were processed by 10X's Cell Ranger version 3.1.0 using the mm10 reference genome, resulting in a filtered HDF5 file. For bulk RNA-seq, sorted cells were used to prepare RNA sequencing libraries by the Epigenomics Core at Weill Cornell Medicine, using the Clontech SMARTer Ultra Low Input RNA Kit V4 (Clontech Laboratories). Sequencing was performed on an Illumina HiSeq 4000, yielding 50-bp single-end reads.

#### Data analysis

For flow cytometry data analysis, we utilized FlowJo (version 10.7.1 and 10.8.0), and numerical data were exported to Excel (Version 16.83) and further analyzed using GraphPad Prism (version 8 or 10) to generate graphical representations and for statistical analysis.

For scRNaseq analysis, data were processed and analyzed using R version 4.2.2 and Seurat package version 4.3.0. Seurat objects were created using only genes appearing in at least 3 cells and cells. Read counts were normalized within each sample using the NormalizeData function. For each sample, integration features were selected using the SelectIntegrationFeatures function with nfeatures set to 2000. Integration of all samples was then performed using either CCA or rPCA methods. The RunPCA function was then run with npcs set to 20. The graph representing cells with similar expression patterns was generated with the FindNeighbors function using the 20 largest principal components. Cell clusters were generated using the Louvain algorithm implemented by the FindClusters function, selected based on visual inspection of a clustree plot. Unidentifiable clusters and doublets were removed from the dataset. Inference of interactions were carried out with CellphoneDB with 1000 iterations after gene names were converted to human genes using BiomRt. All visualizations of scRNA-seq data were generated using the Seurat, ggplot2, EnhancedVolcano, and Circos packages. Statistics for the violin plots were calculated by unpaired two-tailed Wilcoxon rank-sum test.

For bulk RNAseq, raw sequencing reads were demultiplexed with Illumina CASAVA (v.1.8.2). Adapters were trimmed from reads using FLEXBAR (v.2.4) and reads were aligned to the NCBI GRCh37/hg19 human genome using the STAR aligner (v.2.3.0) with default settings. Reads per gene were counted using Rsubread. Prior to differential expression analysis, genes were prefiltered, keeping only those genes with 50 or more counts in at least two samples. Differential expression analysis was performed using DESeq2 (version 1.20.0) using both site (inflamed/adjacent) and patient ID as factors in the design. A false discovery rate of 0.1 was taken to indicate significance. The volcano plot was generated using dplyr (v. 1.1.3), ggplot2 (v.3.4.3), and ggrepel (v. 0.9.3) in R (v 4.1.2).

For manuscripts utilizing custom algorithms or software that are central to the research but not yet described in published literature, software must be made available to editors and reviewers. We strongly encourage code deposition in a community repository (e.g. GitHub). See the Nature Portfolio [guidelines for submitting code & software](#) for further information.

## Data

Policy information about [availability of data](#)

All manuscripts must include a [data availability statement](#). This statement should provide the following information, where applicable:

- Accession codes, unique identifiers, or web links for publicly available datasets
- A description of any restrictions on data availability
- For clinical datasets or third party data, please ensure that the statement adheres to our [policy](#)

All data necessary to understand and evaluate the conclusions of this paper are provided. Single cell RNA sequencing data has been deposited in the Gene Expression Omnibus database under the accession number GSE229976. Bulk RNA sequencing RNA sequencing data has been deposited under the accession number GSE247742. All other data generated in this study are provided within the article and its Supplementary Information/Source Data file. The shell, R and Python scripts that enabled the main steps of the analyses performed in this project are available on request.

## Research involving human participants, their data, or biological material

Policy information about studies with [human participants or human data](#). See also policy information about [sex, gender \(identity/presentation\), and sexual orientation](#) and [race, ethnicity and racism](#).

Reporting on sex and gender

[All available patient characteristics are provided in Supplementary Table 1 and 2.](#)

Reporting on race, ethnicity, or other socially relevant groupings

[All available patient characteristics are provided in Supplementary Table 1 and 2.](#)

Population characteristics

Human tonsil and surgical resection samples from IBD patients were provided by the Cooperative Human Tissue Network (CHTN), which is funded by the National Cancer Institute. Other investigators may have received specimens from the same patients. Samples were received as entirely de-identified human specimens with diagnoses confirmed by medical records and trained pathologists. This protocol was reviewed by the Weill Cornell Medicine institutional review board and determined to meet the exemption category 4 of HHS 45 CFR 46.104(d). Additional oversight of the Cooperative Human Tissue Network is outlined at [www.chtn.org](http://www.chtn.org). Intestinal biopsies from the colon of individuals with Crohn's disease and sex- and age-matched controls without IBD, were obtained following Institutional Review Board approved protocols from the JRI Live Cell Bank Consortium at Weill Cornell Medicine (protocol number 1503015958). Informed consent was obtained from all subjects. All available patient characteristics are provided in Supplementary Table 1 and 2.

Recruitment

Human tonsil and surgical resection samples from IBD patients were provided by the Cooperative Human Tissue Network (CHTN), which is funded by the National Cancer Institute. This protocol was reviewed by the Weill Cornell Medicine institutional review board and determined to meet the exemption category 4 of HHS 45 CFR 46.104(d). Other samples from humans were from JRI IBD Live Cell Bank Consortium at Weill Cornell Medicine. Diagnoses were confirmed by medical records and trained pathologists. There were no self-selection or other biases which affect the result.

Ethics oversight

Protocol to obtain human Samples from Cooperative Human Tissue Network (CHTN) was reviewed by the Weill Cornell Medicine institutional review board and determined to meet the exemption category 4 of HHS 45 CFR 46.104(d). Human samples from the JRI IBD Live Cell Bank Consortium were collected following informed consent under the protocol number: 1503015958.

Note that full information on the approval of the study protocol must also be provided in the manuscript.

## Field-specific reporting

Please select the one below that is the best fit for your research. If you are not sure, read the appropriate sections before making your selection.

Life sciences

Behavioural & social sciences

Ecological, evolutionary & environmental sciences

For a reference copy of the document with all sections, see [nature.com/documents/nr-reporting-summary-flat.pdf](http://nature.com/documents/nr-reporting-summary-flat.pdf)

# Life sciences study design

All studies must disclose on these points even when the disclosure is negative.

Sample size	Animal sample size estimates were determined using power analysis (power=90% and alpha=0.05) based on the mean and standard deviation from our previous studies and/or pilot studies using at least 3 animals per group.
Data exclusions	No data were excluded from the analyses.
Replication	All attempts at replication of experiments were successful. All experiments were independently performed at least twice to ensure reproducibility.
Randomization	No randomization method was used in animal experiments, because littermate group allocation was performed via animal genotype.
Blinding	The investigators were not blinded to allocation because animals were allocated by genotypes. Also, due to potential cross-contamination between infected and non-infected naive animals.

## Reporting for specific materials, systems and methods

We require information from authors about some types of materials, experimental systems and methods used in many studies. Here, indicate whether each material, system or method listed is relevant to your study. If you are not sure if a list item applies to your research, read the appropriate section before selecting a response.

### Materials & experimental systems

- |                                     |   |
|-------------------------------------|---|
| n/a                                 | Involved in the study   |
| <input type="checkbox"/>            | <input checked="" type="checkbox"/> Antibodies                  |
| <input checked="" type="checkbox"/> | <input type="checkbox"/> Eukaryotic cell lines                  |
| <input checked="" type="checkbox"/> | <input type="checkbox"/> Palaeontology and archaeology          |
| <input type="checkbox"/>            | <input checked="" type="checkbox"/> Animals and other organisms |
| <input checked="" type="checkbox"/> | <input type="checkbox"/> Clinical data                          |
| <input checked="" type="checkbox"/> | <input type="checkbox"/> Dual use research of concern           |
| <input type="checkbox"/>            | <input checked="" type="checkbox"/> Plants                      |

### Methods

- |                                     |  |
|-------------------------------------|--|
| n/a                                 | Involved in the study                              |
| <input checked="" type="checkbox"/> | <input type="checkbox"/> ChIP-seq                  |
| <input type="checkbox"/>            | <input checked="" type="checkbox"/> Flow cytometry |
| <input checked="" type="checkbox"/> | <input type="checkbox"/> MRI-based neuroimaging    |

## Antibodies

### Antibodies used

The antibodies are described below. All antibodies were purchased from BD Biosciences, Thermo Fisher, and Biolegend. All antibodies were validated by manufacturers and in previous publications.

Antibodies for mouse flow cytometry:

B220/RA3-6B2/APC-eF780 or Percp-Cy5.5/Thermo Fisher/<https://www.thermofisher.com/antibody/product/CD45R-B220-Antibody-clone-RA3-6B2-Monoclonal/47-0452-82> or <https://www.biologend.com/en-us/search-results/percp-cyanine5-5-anti-mouse-human-cd45r-b220-antibody-4267>

CCR6/29-2L17/BV605 or PE/Biolegend/<https://www.biologend.com/en-us/products/brilliant-violet-605-anti-mouse-cd196-ccr6-antibody-8870?GroupID=BLG7289> or <https://www.biologend.com/en-us/products/pe-anti-mouse-cd196-ccr6-antibody-5220>

CD3ε/145-2C11/Percp-Cy5.5/Thermo Fisher/<https://www.thermofisher.com/antibody/product/CD3e-Antibody-clone-145-2C11-Monoclonal/45-0031-82>

CD4/GK1.5/BUV395 /Thermo Fisher/<https://www.bdbiosciences.com/us/applications/research/t-cell-immunology/th-1-cells/surface-markers/mouse/buv395-rat-anti-mouse-cd4-gk15/p/563790>

CD4/GK1.5/BV605/Biolegend/<https://www.biologend.com/en-us/products/brilliant-violet-605-anti-mouse-cd4-antibody-10708>

CD4/RM4-5/PE/Dazzle 394/ Biolegend/<https://www.biologend.com/en-us/search-results/pe-dazzle-594-anti-mouse-cd4-antibody-9845>

CD5/53-7.3/Percp-Cy5.5/Thermo Fisher/<https://www.thermofisher.com/antibody/product/CD5-Antibody-clone-53-7-3-Monoclonal/45-0051-82>

CD8a/53-6.7/Percp-Cy5.5/Thermo Fisher/<https://www.thermofisher.com/antibody/product/CD8a-Antibody-clone-53-6-7-Monoclonal/45-0081-82>

CD11b/M1/70/APC-eF780/Thermo Fisher/<https://www.thermofisher.com/antibody/product/CD11b-Antibody-clone-M1-70-Monoclonal/47-0112-82>

CD11c/N418/APC-eF780 or FITC /Thermo Fisher/<https://www.thermofisher.com/antibody/product/CD11c-Antibody-clone-N418-Monoclonal/47-0114-82> or <https://www.thermofisher.com/antibody/product/CD11c-Antibody-clone-N418-Monoclonal/11-0114-85>

CD11c/HL3/BD Bioscience/<https://www.bdbiosciences.com/en-us/products/reagents/flow-cytometry-reagents/research-reagents-single-color-antibodies-rou/buv395-hamster-anti-mouse-cd11c.564080>

CD19/eBio1D3/PE-Cy7 or Percp-Cy5.5 /Thermo Fisher/<https://www.thermofisher.com/antibody/product/CD19-Antibody-clone-eBio1D3-1D3-Monoclonal/25-0193-82> or <https://www.thermofisher.com/antibody/product/CD19-Antibody-clone-eBio1D3-1D3-Monoclonal/45-0193-82>

CD45/30-F11/BV785/Biolegend/<https://www.biologend.com/en-us/products/brilliant-violet-785-anti-mouse-cd45-antibody-10636>

CD45/30-F11/BV605/Biolegend/<https://www.biologend.com/en-us/products/brilliant-violet-605-anti-mouse-cd45-antibody-8721>

CD64/X54-5/7.1/BV421/Biolegend/<https://www.biologend.com/en-us/products/brilliant-violet-421-anti-mouse-cd64-fcgammari-antibody-8992>

CD90.2/30-H12/AF700/Biolegend/<https://www.biolegend.com/en-us/products/alexa-fluor-700-anti-mouse-cd90-2-antibody-3412>  
 CD127/A7R34/PE-Cy7 or PE-Cy5/Biolegend/<https://www.biolegend.com/en-us/products/pe-cy7-anti-mouse-cd127-il-7ralpha-antibody-6192> or <https://www.biolegend.com/en-us/products/pe-cyanine5-anti-mouse-cd127-il-7ralpha-antibody-6193>  
 MHC II/M5/114.15.2/eF450/Thermo Fisher/<https://www.thermofisher.com/antibody/product/MHC-Class-II-I-A-I-E-Antibody-clone-M5-114-15-2-Monoclonal/48-5321-82>  
 MHC II/M5/114.15.2/BV650/Biolegend/<https://www.biolegend.com/en-us/products/brilliant-violet-650-anti-mouse-i-a-i-e-antibody-12085>  
 NK1.1/PK136/Percp-Cy5.5/Thermo Fisher/<https://www.thermofisher.com/antibody/product/NK1-1-Antibody-clone-PK136-Monoclonal/45-5941-82>  
 TCR $\beta$ /H57-597/APC-eF780/Thermo Fisher/<https://www.thermofisher.com/antibody/product/TCR-beta-Antibody-clone-H57-597-Monoclonal/47-5961-82>  
 Foxp3/FJK-16S/eF450/Thermo Fisher/<https://www.thermofisher.com/antibody/product/FOXP3-Antibody-clone-FJK-16s-Monoclonal/11-5773-82>  
 IFNy /XMG1.2/BV421/Biolegend/<https://www.biolegend.com/en-us/products/brilliant-violet-421-anti-mouse-ifn-gamma-antibody-7154>  
 IL-17A/eBio17B7/AF488/Thermo Fisher/<https://www.thermofisher.com/antibody/product/IL-17A-Antibody-clone-eBio17B7-Monoclonal/11-7177-81>  
 IL-22/IL22JOP/APC/Thermo Fisher/<https://www.thermofisher.com/antibody/product/IL-22-Antibody-clone-IL22JOP-Monoclonal/17-7222-82>  
 ROR $\gamma$ t/B2D/PE-eF610/Thermo Fisher/<https://www.thermofisher.com/antibody/product/ROR-gamma-t-Antibody-clone-B2D-Monoclonal/61-6981-82>  
 T-bet/eBio4B10/ef660/Thermo Fisher/<https://www.thermofisher.com/antibody/product/T-bet-Antibody-clone-eBio4B10-4B10-Monoclonal/50-5825-82>  
 Ki-67/SolA15/FITC/Thermo Fisher/<https://www.thermofisher.com/antibody/product/Ki-67-Antibody-clone-SolA15-Monoclonal/11-5698-82>  
 Ly6G/1A8/BUV395/BD Biosciences/<https://www.bdbiosciences.com/en-us/products/reagents/flow-cytometry-reagents/research-reagents/single-color-antibodies-ruo/buv395-rat-anti-mouse-ly-6g.563978>  
 Ly6G/1A8/PE-Cy7/Biolegend/<https://www.biolegend.com/en-us/products/pe-cyanine7-anti-mouse-ly-6g-antibody-6139>  
 TCRgd/GL3/Percp-Cy5.5/Biolegend/<https://www.biolegend.com/en-us/products/percp-cyanine5-5-anti-mouse-tcr-gamma-delta-antibody-6702>  
 F4/80/BM8/APC-Cy7/Biolegend/<https://www.biolegend.com/en-us/search-results/apc-cyanine7-anti-mouse-f4-80-antibody-4072>  
 NKp46/29A1.4/PE/Biolegend/<https://www.biolegend.com/en-us/products/pe-anti-mouse-cd335-nkp46-antibody-6523>  
 KLRG1/2F1/KLRG1/APC or FITC/Biolegend/<https://www.biolegend.com/en-us/products/apc-anti-mouse-human-krlg1-mafa-antibody-6866> or <https://www.biolegend.com/en-us/search-results/fitc-anti-mouse-human-krlg1-mafa-antibody-6865>  
 Gata3/L50-823/BUV395/BD Biosciences/<https://www.bdbiosciences.com/en-us/products/reagents/flow-cytometry-reagents/research-reagents/single-color-antibodies-ruo/buv395-mouse-anti-gata3.565448>  
 CTLA-4/UC10-4B9/PE/Thermo Fisher/<https://www.thermofisher.com/antibody/product/CD152-CTLA-4-Antibody-clone-UC10-4B9-Monoclonal/12-1522-82>  
 CD80/16-10A1/FITC/Biolegend/<https://www.biolegend.com/en-us/products/fitc-anti-mouse-cd80-antibody-41>  
 CD86/GL-1/PE/Biolegend/<https://www.biolegend.com/en-us/products/pe-anti-mouse-cd86-antibody-256>  
 PD-L1/1-111A/Thermo Fisher/<https://www.thermofisher.com/antibody/product/CD274-PD-L1-B7-H1-Antibody-clone-1-111A-Monoclonal/13-9971-81>  
 PD-L1/10F-9G2/BV650/Biolegend/<https://www.biolegend.com/nl-nl/products/brilliant-violet-650-anti-mouse-cd274-b7-h1-pd-l1-antibody-16055>

All mouse antibodies were used at 1:200, except for CCR6, NKp46 and CTLA-4 which were used at 1:100.  
 All antibodies information (including catalog number and validation data) can be easily found via the vendor websites.

For human surface staining:

CD45/HI30/BV605/<https://www.biolegend.com/en-us/products/brilliant-violet-605-anti-human-cd45-antibody-8521>  
 CD19/HIB19/FITC/<https://www.thermofisher.com/antibody/product/CD19-Antibody-clone-HIB19-Monoclonal/11-0199-42>  
 CD94/DX22/FITC/<https://www.thermofisher.com/antibody/product/CD94-Antibody-clone-DX22-Monoclonal/11-0949-42>  
 CD34/581/FITC/<https://www.thermofisher.com/antibody/product/CD34-Antibody-clone-581-Monoclonal/CD34-581-01?pluginName=CD14/M5E2/FITC>  
<https://www.thermofisher.com/antibody/product/CD14-Antibody-clone-TuK4-Monoclonal/MHCD1401>  
 CD123/6H6/FITC/<https://www.thermofisher.com/antibody/product/CD123-Antibody-clone-6H6-Monoclonal/11-1239-42>  
 Fc $\epsilon$ R1/AER-37(CRA1- FITC/[https://www.thermofisher.com/antibody/product/Fc \$\epsilon\$ R1-alpha-Antibody-clone-AER-37-CRA1-Monoclonal/11-5899-42](https://www.thermofisher.com/antibody/product/Fc<math>\epsilon</math>R1-alpha-Antibody-clone-AER-37-CRA1-Monoclonal/11-5899-42)  
 CD11c/S-HCL-3/APC-Cy7/<https://www.biolegend.com/en-us/products/apc-fire-750-anti-human-cd11c-antibody-14049?GroupID=BLG15277>  
 CD80/B7-1/BUV737/<https://www.bdbiosciences.com/en-us/products/reagents/flow-cytometry-reagents/research-reagents/single-color-antibodies-ruo/buv737-mouse-anti-human-cd80-b7-1.568364>  
 CD86/IT2.2/BV711/<https://www.biolegend.com/en-us/products/brilliant-violet-711-anti-human-cd86-antibody-11985>  
 PD-L1/27E2A3/BV421/<https://www.biolegend.com/de-at/products/brilliant-violet-421-anti-human-cd274-b7-h1-pd-l1-antibody-7261>  
 MHCII (HLA-DR)/L2423/PerCP-Cy5.5/<https://www.biolegend.com/ja-jp/products/percp-cyanine5-5-anti-human-hla-dr-antibody-4246>  
 CD127/A019D5/PE-Cy7/<https://www.biolegend.com/en-us/products/pe-cyanine7-anti-human-cd127-il-7ralpha-antibody-7216?GroupID=BLG9274>  
 CD3/UCHT1/AF700/<https://www.biolegend.com/en-us/products/alexa-fluor-700-anti-human-cd3-antibody-3394>  
 CD4/SK3/BUV395/<https://www.bdbiosciences.com/en-us/products/reagents/flow-cytometry-reagents/research-reagents/single-color-antibodies-ruo/buv395-mouse-anti-human-cd4.563550>  
 For human intracellular staining:  
 ROR $\gamma$ t/Q21-559/Af647/<https://www.bdbiosciences.com/en-us/products/reagents/flow-cytometry-reagents/research-reagents/single-color-antibodies-ruo/alexa-fluor-647-mouse-anti-human-ror-t.563620>  
 FOXP3/PCH101/PE-eF610/<https://www.thermofisher.com/antibody/product/FOXP3-Antibody-clone-PCH101->

Monoclonal/61-4776-42  
 CTLA-4/14D3/PE/https://www.thermofisher.com/antibody/product/CD152-CTLA-4-Antibody-clone-14D3-Monoclonal/12-1529-42

All human antibodies were used at 1:200 except for CD45, CTLA-4 and ROR $\gamma$  which were used at 1:100. All antibodies information (including catalog number and validation data) can be easily found via the vendor websites.

## Validation

All antibodies used in this study are commercially available and have been validated by the manufacturers' and/or previous publications. These results can be found at the associated links above.

## Animals and other research organisms

Policy information about [studies involving animals](#); [ARRIVE guidelines](#) recommended for reporting animal research, and [Sex and Gender in Research](#)

### Laboratory animals

C57BL/6, Rag1 $^{-/-}$ , IL-23R-eGFP KI (JAX 035863) mice on a C57BL/6 background were purchased from the Jackson Laboratory and used at 6–12 weeks of age. ROR $\gamma$ cre mice on a C57BL/6 background were provided by Dr. Gerard Eberl (Institut Pasteur). C57BL/6 Ncr1cre mice were provided by Dr. Eric Vivier and Ctl4-floxed were provided by Dr. Shimon Sakaguchi. Germ free mice were maintained at the gnotobiotic facility at Weill Cornell Medicine. Both female and male mice were used in this study. All transgenic mice were bred and maintained in specific pathogen free facilities with a 12-hour light–dark cycle, an average ambient temperature of 21°C and an average humidity of 48% at Weill Cornell Medicine. Littermates were used as controls, and sex- and age-matched mice were used in all experiments. In any of these experiments sex was not found to influence the outcome of the results. No mice were excluded from the analysis unless clearly indicated. All experiments were approved and performed according to the Institutional Animal Care and Use Committee guidelines at Weill Cornell Medicine.

### Wild animals

No wild animals were used in this study.

### Reporting on sex

Both male and female mice were used in all studies as no sex differences were observed.

### Field-collected samples

No field-collected samples were used in this study.

### Ethics oversight

All experimental procedures performed on mice in this study are in accordance with guidelines of National Institute of Health (NIH) and the Institutional Animal Care and Use Committee (IACUC) at Weill Cornell Medicine.

Note that full information on the approval of the study protocol must also be provided in the manuscript.

## Flow Cytometry

### Plots

Confirm that:

- The axis labels state the marker and fluorochrome used (e.g. CD4-FITC).
- The axis scales are clearly visible. Include numbers along axes only for bottom left plot of group (a 'group' is an analysis of identical markers).
- All plots are contour plots with outliers or pseudocolor plots.
- A numerical value for number of cells or percentage (with statistics) is provided.

### Methodology

#### Sample preparation

Whole intestines were aseptically removed from the mice and cleaned by removing the fat tissues. For small intestine, Peyer's patches were carefully removed. Afterwards, intestines were opened longitudinally, extensively cleaned with cold Dulbecco's PBS (Corning) and cut approximately into 0.5 cm sections. To dissociate epithelial cells, cut tissues were incubated in Hanks' balanced salt solution containing 5 mM EDTA (Thermo Fisher Scientific), 1 mM dithiothreitol (Sigma-Aldrich) and 2% fetal bovine serum twice at 37 °C for 20 minutes. After incubation, the tissues were vortexed, transferred to digestion buffer containing collagenase III (1 mg mL $^{-1}$ ; Worthington), dispase (0.4 U mL $^{-1}$ ; Thermo Fisher Scientific), DNase I (20  $\mu$ g mL $^{-1}$ ; Sigma-Aldrich) and 10% FBS in RPMI 1640 (Corning), and incubated in a shaker at 200 rpm for 1 hour at 37°C. Leukocytes were enriched by 40/80% density gradient Percoll centrifugation (GE Healthcare).

Human surgical intestinal samples were incubated with continuous shaking in PBS containing 5% FBS, 1 mM EDTA and 1 mM DTT for 30 minutes at 37 °C to remove the epithelial cells. After incubation, the tissues were vortexed, similarly transferred to digestion buffer containing 2 mg/mL Collagenase D (Sigma) and 0.1 ug/mL DNase I (Sigma) in RPMI 1640 (Corning) with 5% FBS for 1 hour. After digestion, the single cell suspension was passed through a 70  $\mu$ m cell strainer to obtain the cells. Further, the cells were immediately cryopreserved for future use with side-by-side analyses.

#### Instrument

5 laser, 18 color BD LSRII (BD) or 5 laser, 18 color FACSAria III

#### Software

FlowJo (version 10.7.1 and 10.8.0), Excel (Version 16.83), and GraphPad Prism (version 8 or 10)

#### Cell population abundance

The purities of sorted cells were more than 97%, cell sorter (FACSAria II) performance assessed before each sorting run using

Cell population abundance	CS&T beads as per manufacturers instructions. Populations of interest were identified after exclusion of dead cells and doublets to maximize the purity.
Gating strategy	For all experiments, cells were first identified by SSC-A/FSC-A scatter gating and single cells based on SSC-H/SSC-A and FSC-H/FCS-A. Dead cells were then excluded based on the absence of fixable live/dead viability dye. Immune cells were then identified by the positive staining of CD45 marker. Detailed gating strategies specific cell populations are provided in the Extended Data Figures.

Tick this box to confirm that a figure exemplifying the gating strategy is provided in the Supplementary Information.